Introduction to Environmental Remote Sensing

BSRSI

Produced for:

Basic Science and Remote Sensing Initiative

Department of Geography

Michigan State University

Introduction to Environmental Remote Sensing

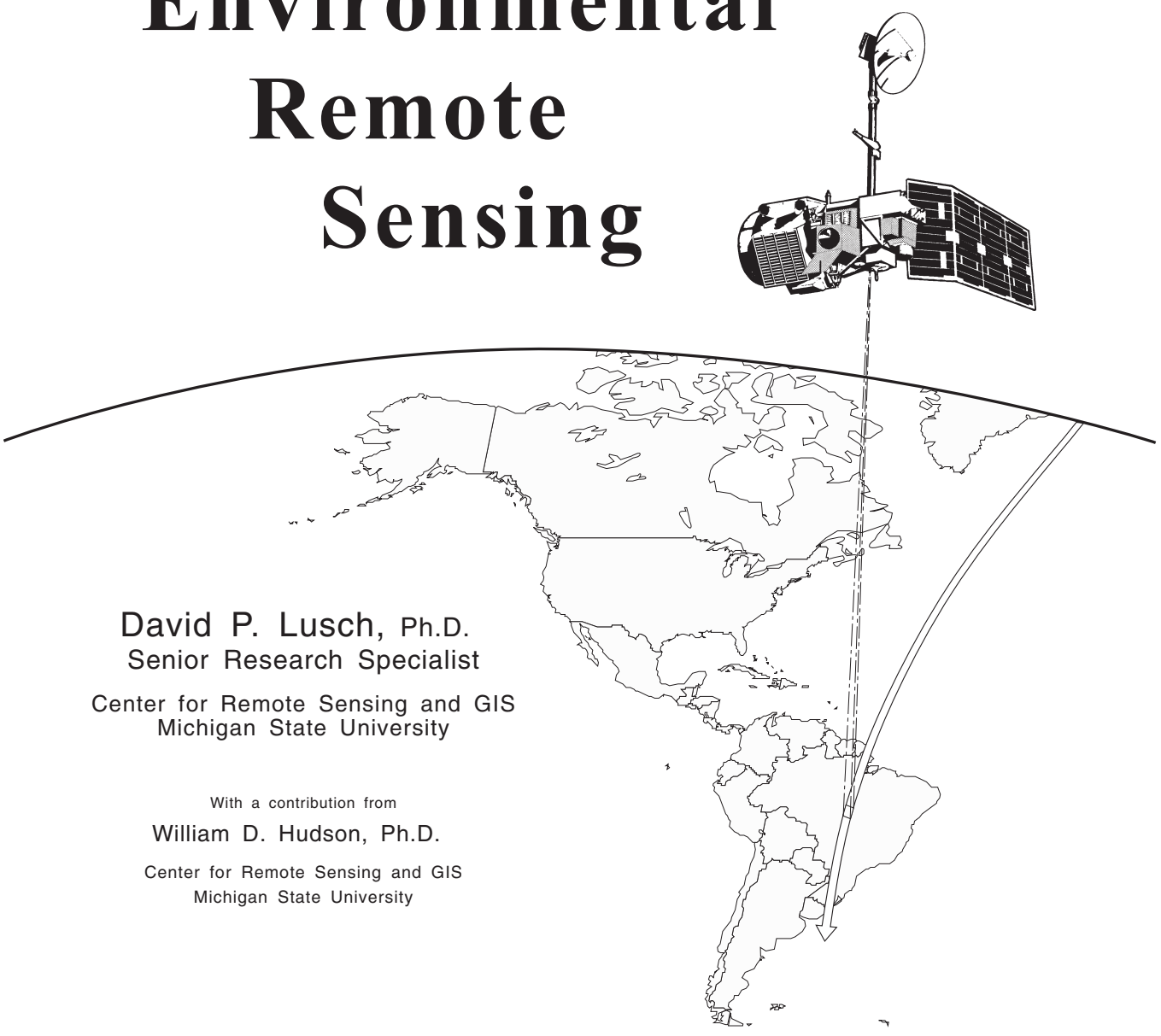

David P. Lusch, Ph.D.
Senior Research Specialist

Center for Remote Sensing and GIS
Michigan State University

With a contribution from

William D. Hudson, Ph.D.

Center for Remote Sensing and GIS
Michigan State University

Graphics and Layout

George F. Weisenborn, IV
Paul Rindfleisch
Michael D. Hyslop

© 1999 David P. Lusch, Ph.D

© 1999 David P. Lusch, Ph.D.

Chapter 1	Introduction to Remote Sensing

Contents

© 1999 David P. Lusch, Ph.D.

1.1 Objectives

- Define remote sensing
- Explain the relationship of airphoto interpretation to remote sensing
- Review the increasing pace of technological development in remote sensing since the launch of Landsat 1
- List at least five current satellite-based remote sensing systems
- Define the "multi-" concept of remote sensing and describe at least four examples

1.2 Introduction

Remote Sensing is a multi-disciplinary technique of electronic and analog image acquisition and exploitation which includes aerial photography and airphoto interpretation.

It has as its goal: "...the measurement or acquisition of information about some property of an object or phenomenon by a recording device which is not in physical or intimate contact with the object or phenomenon under study..." (Manual of Remote Sensing, 1983)

remote: separated by great intervals

sensing: to detect or characterize

[Remote sensing = detect / characterize at a distance]

Inherent aspects of the above definition:

- data collection
- data analysis

The basic concept of remote sensing is the ability to measure spatial, spectral, and temporal variations.

Spatial — variations in scale / size
Spectral — variations in reflected or emitted radiation
Temporal — variations over time (diurnal, seasonal, annual, etc.)

© 1999 David P. Lusch, Ph.D.

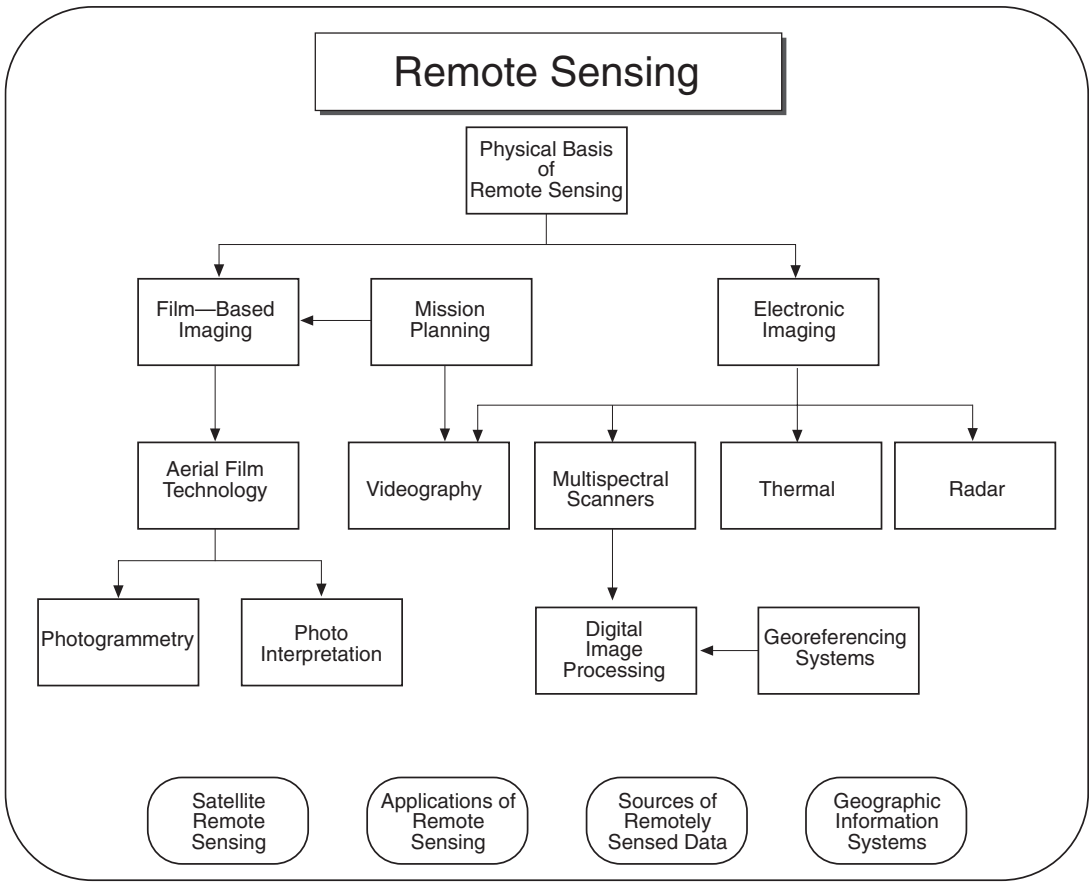

© 1999 David P. Lusch, Ph.D.

1.3 Historical Perspective

1839 — Louis J. M. Daguerre of Paris developed a process for making a photograph

1858 — aerial photographs, taken from balloons, used for mapping and military reconnaissance

45 years

1903 — Wright brothers' first flight

WW I and WW II — major developments for military aerial reconnaissance

1930's — USDA begins extensive photography programs for civilian uses

1950's — photogrammetry and photointerpretation firmly institutionalized into a variety of disciplines

1960's — remote sensing is born from the "space age"

1.4 Development of Photography

1038 In his book on optics, Alhazen describes the camera obscura

1568 Daniello Barbaro of Venice used a lens in the camera obscura

1727 During his experiments concerning the production of phosphorous, Johann Schulze discovers that white chalk moistened with a silver nitrate solution in nitric acid darkened in sunlight

1802 Thomas Wedgwood and Sir Humphrey Davy described a method of producing images (temporarily) on paper coated with nitrate or silver chloride

1822 Joseph Niepce makes the first permanent photographic images on paper coated with silver chloride

1831 Louis Daguerre discovers that silver iodide is photosensitive and that a latent image can be made visible by subjecting the metal photographic plate to mercury vapors

© 1999 David P. Lusch, Ph.D.

1834 The English scientist William Talbot invented the negative-positive photographic process

1839 Daguerre perfects and publishes his daguerreotype process which utilized sodium thiosulphate as a fixer. The English chemist and astronomer Sir John Herschel had discovered sodium thiosulphate in 1819

1847 Claude De St. Victor succeeds in producing a negative on glass

1851 Frederick Archer invented the wet collodian process. The light-sensitive material had to be prepared just before the intended exposure and had to processed immediately afterwards

1871 Richard Maddox, an English physician, produced the first practical silver-bromide gelatin negatives on glass thereby freeing photographers from having to make their own wet plates

1883 George Eastman invented paper roll films, replacing glass plates

1891 Gabriel Lippmann published his method of interference-color photography

1936 Eastman Kodak Company and Agfa introduced commercially available color film

1.5 Development of Aerial Photography

1783 **June** *Joseph and Etienne Montgolfier* demonstrated the flight of an unmanned, hot-air balloon which attained an altitude of 6,000 feet

August *J.A.C. Charles*, a noted French physicist, launched the first hydrogen-filled balloon in an unmanned ascent over the Champ de Mar in Paris

December *Charles* and a passenger ascended from the Tuileries Gardens in a hydrogen-filled balloon remaining aloft for nearly two hours and travelling 27 miles

1785 *Jean Blanchard*, a Frenchman, and John Jefferies, an American, made the first aerial crossing of the English Channel from

© 1999 David P. Lusch, Ph.D.

Dover to Calais in a balloon

1858 *Gaspard Tournachon* (Nadar) made the first aerial photograph of Paris from a balloon tethered at an altitude of 80 meters

1860 *James Black* and *Samuel King* ascended to an altitude of 630 meters and successfully photographed parts of the city of Boston

1882 The English meteorologist *E.D. Archibald* made the first successful aerial photographs from a kite

1885 Some of the earliest vertical air photos from balloons were made by *Gaston Tissandier* and *Jacques Ducom*

1898 During the Spanish-American War, American troops tried unsuccessfully to utilize balloon photography for tactical reconnaissance

1903 *Orville* and *Wilbur Wrigh*t fly the first heavier-than-air aircraft at Kill Devil Hill, North Carolina

Julius Neubronner patented a breast-mounted aerial camera for carrier pigeons

1906 *George Lawrence* obtained a 1.35 x 2.4 meter picture of San Francisco during the earthquake. His 1,000 pound camera was suspended at an altitude of 610 meters from a battery of 17 kites

1909 April 24 The first aerial photograph from an airplane was taken over Centocelli, Italy. *Wilbur Wright* was the pilot

1914-1918 Aerial photography played a decisive role as a tactical reconnaissance tool during World War I

1920 *Sherman Fairchild* designed and built the K-3 aerial camera which incorporated an interlens shutter, motor drive and intervalometer

1925 November 20 *Lt. George W. Goddard* acquired the first night-time airphoto over Rochester, New York using a flash bomb and photocell-actuated shutter

1934 The American Society of Photogrammetry was formed

1937 USDA-FSA began photographing selected counties in the

© 1999 David P. Lusch, Ph.D.

U.S. on a repetitive basis
1939-1945 Aerial reconnaissance during World War II provided over 90% of all the intelligence information to the Allies

1942 Eastman Kodak Company introduced Kodacolor Aero Reversal Film.

Under the auspices of the Camouflage Section, National Defense Research Committee, the Eastman Kodak Research Laboratories developed a false-color, camouflage-detection film by modifying the blue, green, red sensitivities of Kodacolor Aero film to green, red and infrared [color infrared (CIR) film]

1950's Photogrammetry and photointerpretation become firmly institutionalized in a variety of disciplines

1.6 Development of Remote Sensing

1960's As the techniques to record electromagnetic radiation beyond the range of human vision became available, the new term "remote sensing" was coined by *Evelyn Pruitt* at the Office of Naval Research to encompass the total observational process from remote platforms

1962 **October** High-Altitude aerial photographs from U-2 aircraft documented the emplacement of Soviet medium-range ballistic missiles in Cuba

1965 Multispectral camera systems (multiband photography) become commercially available

1969 **March** SO 65 Multispectral Photographic Experiment was flown onboard Apollo 9

June NASA's Manned Spacecraft Center begins high-altitude aerial photography missions as part of the Earth Resources Program

1972 **July 23** The Earth Resources Technology Satellite (ERTS-1) was launched. Later renamed Landsat 1

1973 **May 14** Skylab was launched and between May 25, 1973 and February 8, 1974 was occupied for a total of 171 days by 3 different three-person crews. Using the Earth Resources Experiment Package (EREP), these astronauts were able to synoptically survey selected areas of the globe. Skylab reentered the earth's atmosphere on July 11, 1979 and broke-up over the Indian Ocean

© 1999 David P. Lusch, Ph.D.

1975 January 22 Landsat 2 was launched and nine day repetitive coverage becomes possible

1978 January 6 Landsat 1 was retired after acquiring more than 270,000 scenes of data

March 5 Landsat 3 was launched

June 26 Seasat 1 was launched, but suffered a complete system failure on October 10, 1978

October 13 TIROS-N was launched

1979 June 27 NOAA-6 was launched

1981 June 23 NOAA-7 was launched

November 12-14 SIR-A experiment conducted from Space Shuttle Columbia. 10 million km^2 of SAR image coverage collected

1982 Landsat 4 is launched. Onboard is a new sensor - Thematic Mapper (TM) which provides 7 spectral channels and 30 meter resolution (120 IFOV on the thermal band)

1984 March 1 Landsat 5 was launched ahead of schedule due to equipment problems with Landsat 4

October 4-13 SIR-B experiment conducted from Space Shuttle Challenger

December 12 NOAA-9 was launched

1985 The American Society of Photogrammetry (ASP) is renamed the American Society of Photogrammetry and Remote Sensing (ASPRS)

1986 February 21 SPOT-1 was launched from Kourou, French Guiana. Onboard were new sensors which pioneered "pushbroom" scanning using arrays of CCD detectors. One panchromatic band (10 m spatial resolution) and 3 multispectral bands (20 m spatial resolution) were provided. Operational stereo imagery from space became possible.

September 17 NOAA-10 was launched.

© 1999 David P. Lusch, Ph.D.

1987 **February 19** MOS-1 (Marine Observation Satellite), Japan's first earth-resources remote sensing spacecraft, was launched

1988 **September 24** NOAA-11 was launched

1990 **January 22** SPOT-2 was launched

February 7 MOS-1b was launched

December 31 SPOT-1 retired from active service

1991 **May 14** NOAA-12 was launched

July 17 ERS-1 was launched from Kourou, French Guiana. Operational space-borne SAR imagery begins

August 29 IRS-1B, featuring blue, green, red, and NIR sensors and two different ground resolutions (36m and 72m), was launched

1992 **February 11** JERS-1 featuring an 18m by18m resolution synthetic aperture radar (SAR) sensor and a 7 band, 17m by 24m optical sensor, was launched.

August 20 Topex/Posieden, with the mission of detecting minute (~5cm) sea level changes using French and American made altimeters, was launched.

1993 **September 26** SPOT-3 was launched.

1994 **October 15** IRS-P2 was launched.

November 4 RESURS 01-3, a Russian satellite with the mission of gathering mapping scale data, and large scale measurement and monitoring of agriculture, forestry, coastal zones, ice and snow, was launched.

1995 **April 21** ERS-2 was launched..

November 4 RADARSAT, a Canadian satellite featuring a SAR system with variable look angles, resolutions, and swath widths, was launched.

December 28 IRS-1C with a 5m resolution panchromatic band and wide angle viewing capabilities was launched.

© 1999 David P. Lusch, Ph.D.

1996 March 21 IRS-P3 was launched

August 17 ADEOS - 1, a Japanese made satellite with instrumentation including a five band visible/NIR radiometer (AVNIR) with stereo and pointable capability, a scatterometer to measure wind speed and direction over the world's oceans (NSCAT), an ozone detector (TOMS), and ocean color and temperature detector (OCTS) was launched.

1997 June 30 Communications with ADEOS - 1 were lost.

August 1 Seastar satellite with the SeaWifs multispectral sensor for taking ocean color measurements was launched.

August 22 LEWIS commercial (TRW Space and Electronics Group) satellite with a 30m resolution , 364 channel hyperspectral imager, and 300m resolution, 256-spectral-channel Linear Etalon Imaging Spectral Array, was launched.

August 28 LEWIS satellite began a slow spin which ultimately lead to complete power loss and a decaying orbit.

September 29 IRS-1D featuring a 5 day repeat cycle on its wide angle and panchromatic instruments, and the LISS 3 instrument were launched.

December 24 Early Bird satellite, a commercial (Earth Watch Inc.) satellite with 0.82m resolution in panchromatic and 3.82m resolution in color wavelengths, and high revisit frequency was launched.

December 28 Communication with EarlyBird satellite was lost.

1998 March 24 SPOT-4 carrying dual HRVIR instruments which include a SWIR band and the VEGETATION instrument was launched.

May13 NOAA-15 was launched.

July INSAT is scheduled to be launched.

November QUIKSCAT, a satellite with a sensor similar to the NSCAT instrument lost on with ADEOS -1 is scheduled to be launched.

© 1999 David P. Lusch, Ph.D.

1999 **April 15** LANDSAT 7 is launched, carrying the ETM+ instrument which features a 15m panchromatic band and a 60m TIR band in addition to its six 30m bands(VIS, NIR & SWIR).

April 22 Ikonos-1, a commercial 1m imaging system, was launched, but failed to achieve orbit.

May Oceansat / IRS-P4 was launched.

September DMSP is scheduled for launch.

September The Shuttle Radar Topography Mission (SRTM) which will use a space borne microwave system and single pass radio interferometry to study Earth surface change and construct three dimensional model of the Earth's surface is scheduled to be launched.

October Terra (EOS AM-1) is scheduled for launch. It includes ASTER, a 4-band multispectral (visible, shortwave IR, and TIR) sensor; CERES, an instrument used to look at clouds and the radiant energy of the Earth; MISR, a 4-band (3 visible, 1 NIR) radiometer capable of obtaining data from multiple angles; MODIS, a 36-band radiometer with coarse spatial resolution but a 1 to 2 day revisit capacity;and MOPITT, an instrument designed to measure atmospheric carbon monoxide and methane concentrations.

November OrbView-3, a commercial 1m system, is scheduled for launch.

December EO-1 is scheduled to be launched. It will carry the Advanced Land Imager, the "new millenium" replacement of ETM+, providing six Landsat bands plus three new ones: 433-453, 845-890 and 1200-1300 nm. Hyperion, a hyperspectral imager providing 220 bands (from 400-2500 nm at 30 resolution) will also be flown on EO-1.

December NOAA-L is scheduled to be launched.

2000 The following systems are scheduled to be launched:

ADEOS-2
IRS-P6
ENVISAT-1
EOS PM-1
JASON-1
Meteosat 8
OrbView 4
Radarsat 2

© 1999 David P. Lusch, Ph.D.

1.7 The "multi" Concept

The ability to acquire a multitude of data and to process these data with multiple analysis techniques has led to the more generalized concept of "multi". A combination of factors are considered collectively, compared to using a single product or technique approach.

- Multistation (vs one station)
- Multiband and Multispectral (vs one wave-length band)
- Multidate (vs one date)
- Multipolarization (vs one polarization)
- Multistage (vsone stage or flight altitude)
- Multidirectional (vertical plus oblique directions)
- Multienhancement (vs one enhancement)
- Multidisciplinary Analysis (vs experts from only one discipline)
- Multithematic (a series of maps, each dedicated to the protraying of one particular theme, rather than through only one map)

(source: U.S. Forest Service: *High Altitude Photography Training Manual*)

c 1999 David P. Lusch, Ph.I

Chapter 2	The BioPhysical Basis of Remote Sensing

Contents

© 1999 David P. Lusch, Ph.D.

2.1 Objectives

- Label the components of the energy flow diagram for passive remote sensing
- Explain the difference between passive and active remote sensing
- Label the major spectral regions on a diagram of the electromagnetic spectrum and define "optical remote sensing"
- Describe the effects of scattering and absorption in the atmosphere
- Define the term "atmospheric window" and list those which are important to optical remote sensing
- Draw the generalized spectral reflectance curve from 0.4 - 2.5 μm for vegetation, soil, and water
- Given a set of spectral reflectance curves, identify the basic earth feature each represents
- Explain how multispectral reflectance measurements could be exploited to discriminate between vegetation, soil, and water features

2.2 Introduction

The physical basis of remote sensing provides the fundamental theories and principles which underlie all subsequent discussions of remote sensing and its many applications. Electromagnetic energy; its source, properties and interactions in the atmosphere, are briefly discussed. The physical controls of the reflectance, absorptance, and transmittance of solar radiation with respect to earth targets is introduced prior to a detailed, target-specific discussion of the relationship between spectral reflectance and certain biophysical attributes. An understanding of the relationships between certain fundamental biophysical attributes and spectral reflectance is a basic prerequisite to comprehending any remotely-sensed scene acquired in the 400-2500 nm wavelength region.

© 1999 David P. Lusch, Ph.D.

2.3 Radiation Terminology

Radiant energy Q units: joules J

Energy traveling in the form of electromagnetic waves.

Radiant flux Φ units: watts W (joules/second)

The rate at which radiant energy is transferred from a point or a surface to another surface; a measure of radiant power.

$$\Phi = dQ / dt$$

Radiant flux density E or M units: watts per sq. meter, Wm^{-2}

The radiant flux at a surface divided by the area of the surface. When referring to the radiant flux *incident on* a surface, we call it:

Irradiance $E = d\Phi / dA$ $[Wm^{-2}]$

When referring to the radiant flux *emitted from* a surface, we call it:

Radiant exitance $M = d\Phi / dA$ $[Wm^{-2}]$

Notice that the units and defining equations for both *radiant exitance* and *irradiance* are identical. The only difference between these two radiometric terms is that *irradiance* refers to radiation *arriving at* a surface, where as *radiant exitance* refers to radiation *leaving* a surface.

Radiant intensity I units: watts per steradian, Wsr^{-1}

Radiant flux proceeding from a source per unit solid angle ($d\Omega$)

$$I = d\Phi / d\Omega$$

Radiance L units: watts per sq. meter and steradian, Wm^{-2} sr^{-1}

Radiant flux propagated in a given direction, per unit solid angle about that direction and per unit area projected normal to the direction ($dA \cos\Theta$). The angle Θ is measured between the direction and a perpendicular to the unit area. Radiance is a geometric radiation quantity that describes the spatial distribution of radiant flux density.

$$L = d^2\Phi \setminus d\Omega\, dA\cos\Theta$$

© 1999 David P. Lusch, Ph.D.

Bidirectional Reflectance Distribution Factor (BRDF)

The BRDF is the ratio of radiant flux reflected by a target *under specified conditions of irradiation and viewing* to that reflected by a near-completely reflecting, almost perfectly diffuse reference surface which is identically irradiated and viewed. A "perfectly diffuse" surface reflects equally in all directions (also called a *Lambertian reflector*). The radiance of a uniformly illuminated Lambertian surface of infinite extent is constant for any viewing angle. If the uniformly illuminated Lambertian surface is small enough so as not to fill the field of view of an observing sensor, the radiance measured by the sensor will be proportional to the cosine of the viewing angle. A "completely reflecting" surface reflects all of the radiant flux falling on it.

The ideal "completely reflecting, perfectly diffuse" surface does not exist, but several useful reference compounds have been developed. Properly prepared *barium sulfate* ($BaSO_4$) or *magnesium oxide* (MgO) reference surfaces closely approximate perfect diffusers for view angles - 45^0. Pressed $BaSO_4$ powder (useful in lab environments only) departs from being "completely reflecting" by less than one percent in the wavelength range 375-1100 nm. Barium sulfate paint (useful in field environments) is almost as good; it departs from the completely reflecting assumption by no more than two percent in the 375-1100 nm wavelength range and is more than 99% reflective from 460-800 nm.

Recently, another compound has been developed as a reference standard which is particularly well-adopted to field conditions. Commonly referred to by the trade name *Halon*, this fluorocarbon resin is *polytetrafluoroethylene (PTFE)*. PTFE closely approximates a perfect diffuser for view angles $<45^0$. Pressed PTFE powder (useful in lab environments only) departs from the "completely reflecting" assumption by less than one percent in the wavelength range 350-1800 nm; it is more than 98% reflective in the wavelength range 280-2000 nm.

Schutt et. al. (1981) reviewed $BaSO_4$ as reflectance standard and noted, "... the IR reflectance of a $BaSO_4$ standard reflectance diffuser is sensitive to changes in humidity, and its reflectance cannot be recovered once it has been soiled. Clearly, applications of $BaSO_4$ are limited under certain environmental conditions outside the laboratory." They tested Halon (PTFE) prepared for spray application and found its reflective properties to be comparable with those of $BsSO_4$ paint. Furthermore, because PTFE is hydrophobic, it is

© 1999 David P. Lusch, Ph.D.

both washable and insensitive to humidity changes. Hence, Schutt et. al. (1981) recommend *Halon (PTFE)* in place of $BaSO_4$ paint as a field reflectance standard.

References:

DeWitt, D. P. and Robinson, B. F. 1976. Description and evaluation of a bidirectional reflectance factor reflectometer. LARS Information Note 091576. Laboratory for Applications of Remote Sensing. Purdue University, West Lafayette, Indiana. 40 p.

Schutt, J. B. et. al. 1981. Reflectivity of TFE — a washable surface —compared with that of $BaSO_4$. *Applied Optics*, v.20, n. 12, pp. 2033-2035.

Weidner, V. R. and Hisa, J. J. 1981. Reflection properties of pressed polytetrafluoroethylene powder. *J. Opt. Soc. Am.*, v. 71, n. 7, pp. 856-861.

2.4 Electromagnetic Energy

Typical energy flow - passive systems (Figure 2.1)

- energy source
- path length
- atmospheric interactions
- target interactions
- energy sensor
- active vs passive remote sensing

Electromagnetic energy

Electromagnetic radiation (EMR) is a dynamic form of energy made manifest only by its interaction with matter. EMR radiates according to the basic wave theory (Figure 2.2) which describes electromagnetic energy as traveling in a harmonic, sinusoidal fashion at the "velocity of light," $c = 3 \times 10^8$ m / sec. Wavelength (λ) is the linear distance between successive peaks, frequency (υ) is the number of peaks passing a fixed point in space per unit time.

$$c = \upsilon \lambda$$

© 1999 David P. Lusch, Ph.D.

Typical Energy Flow 2.1

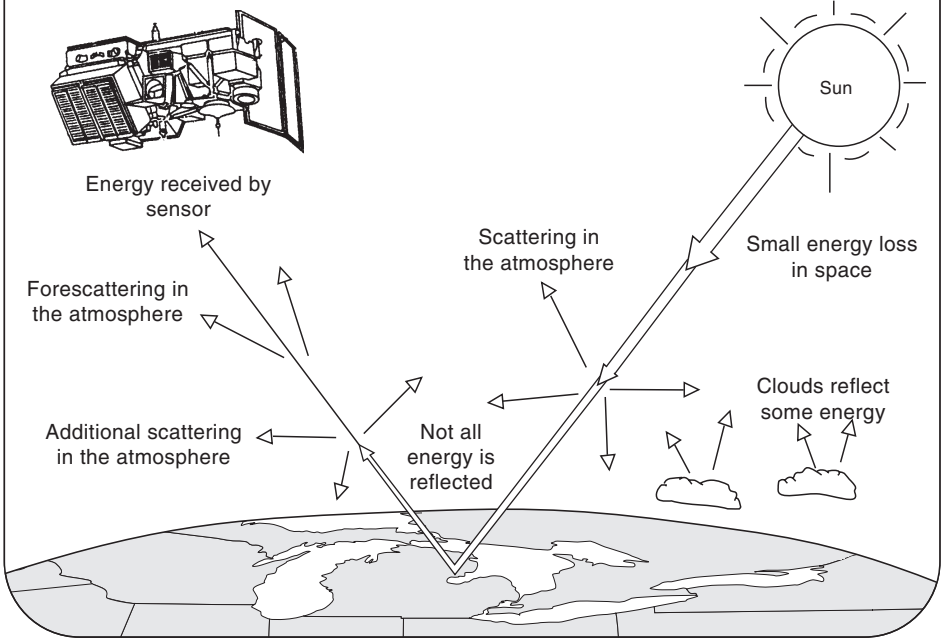

Wave Theory 2.2

$$c = \upsilon \cdot \lambda$$

$$c = 3x10^{8} \text{ ms}$$

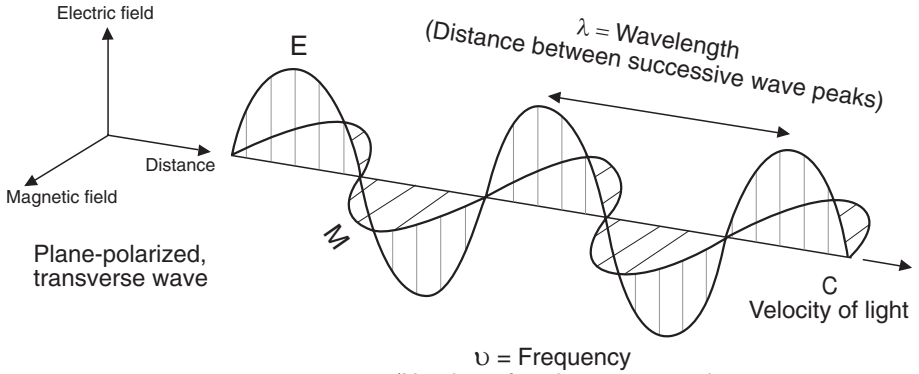

υ = Frequency
(Number of cycles per second passing a fixed point)

© 1999 David P. Lusch, Ph.D.

The *particle theory* describes EMR as being composed of many discrete units called *photons* or *quanta*. The energy of a quantum is given as

$$E = h\upsilon$$

E = energy of a quantum, Joules (J)
h = Planck's constant, 6.626×10^{-34} J sec.

The wave and quantum models of EMR are related by

$$E = \frac{hc}{\lambda}$$

The energy of a quantum is inversely proportional to its wavelength. The longer the wavelength, the lower its energy content. This principle has important implications in remote sensing, particularly with regard to naturally emitted microwave radiation — hence the dominance of active microwave sensors.

The sun is the most obvious source of EMR for remote sensing, but ***ALL*** matter at temperatures above absolute zero (0 K or -273^0C continuously *emit* EMR. The amount of energy emitted is a function of the objects surface temperature as set forth in the *Stefan-Boltzmann Law*.

$$W = \sigma T^4$$

W = total radiant emittance, W / m^2
σ = Stefan-Boltzmann constant,
5.6697×10^{-8} $W / m^2 / K^4$
T = absolute temperature (K)

Total emitted energy varies with the *fourth power* of T and therefore increases very rapidly with increases in temperature.

The spectral distribution of emitted energy also varies with temperature according to Wien's Displacement Law.

$$\lambda_m = \frac{A}{T}$$

λ_m = wavelength of maximum spectral emittance
A = 2898 μm K
T = temperature, K

© 1999 David P. Lusch, Ph.D.

Together, the Stefan-Boltzmann Law and Wein's Law stipulate that:

- the higher the temperature of a radiator, the greater the amount of radiation it emits (area under the curve)

- as temperature increases, the peak of the spectral radiation distribution shifts toward shorter wavelengths

The sun emits EMR in a manner similar to a blackbody radiator at 6,000 K and has its peak spectral energy at about 0.5μm. This corresponds to the peak spectral sensitivity of human eyes.

Electromagnetic Spectrum (Figure 2.3)

• Ultraviolet	$\lambda < 0.4$ μm
• Visible light	$\lambda = 0.4$ to 0.7 μm
• Near IR	$\lambda = 0.7$ to 1.35 μm
- Photographic IR	$\lambda = 0.7$ to 0.98 μm
• Middle IR (SWIR)*	$\lambda = 1.35$ to 3.0 μm
• Thermal IR	$\lambda = 3.0$ to 14.0 μm
• Microwave	$\lambda =$ 1mm to 1m

* Short-Wavelength IR (SWIR)

2.5 Energy Interactions in the Atmosphere

The earth's atmosphere has a profound effect on the intensity and spectral composition of EMR passing through it, principally through the mechanisms of *scattering* and *absorption.*

Scattering is unpredictable diffusion of radiation by particles in the atmosphere (Figure 2.4).

Rayleigh scatter - diffusion of radiation as it interacts with atmospheric constituents the diameters of which are much smaller than the wavelength of the interacting radiation. The *effect of Rayleigh scatter is inversely proportional to the fourth power of wavelength.* Short wavelengths are scattered more than long wavelengths, hence the blue sky. *Haze* is a primary effect of Rayleigh scatter.

© 1999 David P. Lusch, Ph.D.

Electromagnetic Spectrum 2.3

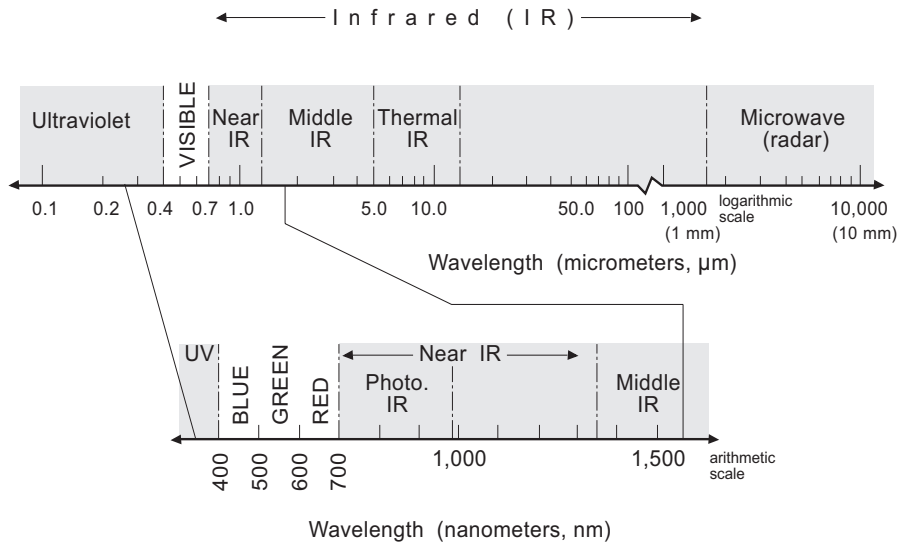

© 1999 David P. Lusch, Ph.D.

Mie scatter - diffusion of radiation by atmospheric particulates having diameters about equal to the wavelength of the interacting radiation. Water vapor and dust are the major causes.

Nonselective scatter - radiation diffusion by atmospheric particles whose diameters are much larger than the energy wavelength. Water droplets, commonly 5 to 100 μm in diameter, scatter all visible and reflective IR wavelengths about equally, hence white clouds.

Absorption - a thermodynamically irreversible transformation of radiant energy into heat.

Atmospheric absorption is due primarily to water vapor, carbon dioxide and ozone. These gases selectively absorb EMR in specific wavelength bands. Wavelength regions in which the atmosphere is particularly transmissive of energy are called *atmospheric windows*.

Figure 2.5 depicts the spectral transmittance of the atmosphere and shows the five "windows" used routinely in remote sensing. These windows are listed below:

Atmospheric Windows

Reflected EMR

- **visible and near infrared** (**0.3-1.3 μm**) very high transmission (several small H_2O absorption features between 0.8 and 1.1 μm)
- **middle infrared** (**1.5-1.8 μm** and **2.0-2.6 μm**) high transmission, but several very strong H_2O and CO_2 absorption bands at 1.4, 1.9, and 2.7 μm

Emitted Thermal IR

- **short-wavelength thermal infrared** (**3.5-5 μm**) popular window for night-time thermal sensing
- **long-wavelength thermal infrared** (**8-14 μm**) most frequently used thermal window

Non-optical EMR

- **microwave** (**> 5.5 mm**) transmission is virtually 100% (between 14 μm and 5.5 mm atmospheric transmission is very low)

© 1999 David P. Lusch, Ph.D.

Atmospheric Scattering 2.4

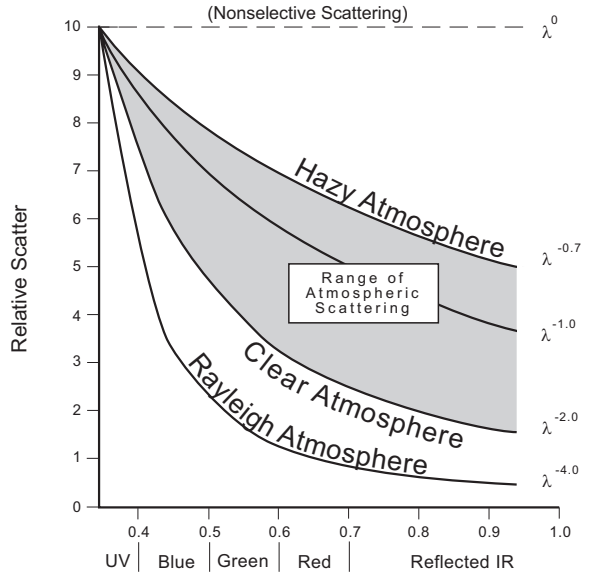

Atmospheric Transmissivity 2.5

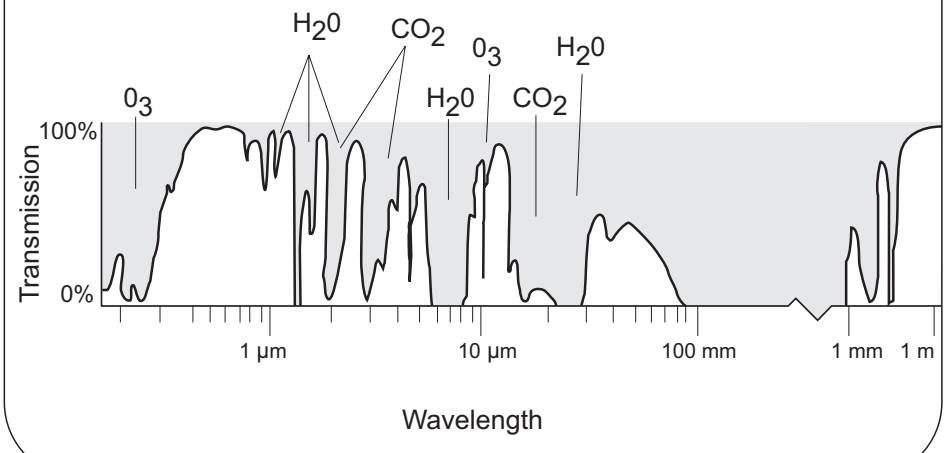

© 1999 David P. Lusch, Ph.D.

ENERGY INTERACTIONS WITH EARTH SURFACE MATERIALS

EMR incident on any earth surface will interact in three fundamental ways - various fractions of the energy will be ***reflected, absorbed and/or transmitted.***

$$E_I(\lambda) = E_R(\lambda) + E_A(\lambda) + E_T(\lambda)$$

E_I = incident energy

E_R = reflected energy

E_A = absorbed energy

E_T = transmitted energy

(λ) = denotes all components are a function of wavelength

Reflection, absorption, and transmission will vary for different earth features and help us to distinguish between them.

The wavelength dependency is critically important because two indistinguishable features in one wavelength region may be very different in another wavelength band - the foundation of multispectral remote sensing.

Specular Reflection - mirror like, where the angle of reflection equals the angle of incidence.

Diffuse Reflection - reflection is uniform in all directions (Lambertian).

EMR absorbed or transmitted by earth features are of little direct use in remote sensing except that the reflected energy we are interested in is reduced by these two mechanisms.

© 1999 David P. Lusch, Ph.D.

Solar Radiant Flux

For our purposes, the sun may be considered as a sphere of gas, nearly 1.4 million kilometers in diameter, which is heated by continuous nuclear reactions at its center. The spectral radiant flux output from the sun is complicated by the tremendous temperature variations which occur along its radius. Also, the solar atmosphere is opaque to certain wavelengths. Stated simply, the effective blackbody temperature (EBT) of the sun is wavelength dependent. In the wavelength region from 350 to 2500 nm, the EBT varies from 5,700 to 6,000 kelvin. At its peak exitance wavelength (487 nm), the sun can be best approximated by a blackbody source at 5,950 kelvin. For general discussion purposes, an average EBT of 6,000 kelvin can be used in the wavelength region 400-2500 nm. As show in Figure 2.6, more than 50 percent of the total solar energy present in the visible through middle-infrared spectrum occurs in the visible light region (400-700 nm).

2.6 Spectral Reflectance Characteristics of Earth Cover Types

BioPhysical Controls of Vegetation Reflectance

Energy Partitioning. From an energy balance viewpoint, all solar radiant flux incident upon any object is either reflected, transmitted, or absorbed. As a group, vegetation is unique in its three-segment partitioning of solar irradiance (Figure 2.7). In the visible part of the spectrum (400-700 nm), reflectance is low, transmittance is nearly zero, and absorptance is high. The fundamental control of energy-matter interactions with vegetation in this part of the spectrum is plant pigmentation.

In the longer wavelengths of the near-infrared portion of the spectrum (700-1350 nm), both reflectance and transmittance are high whereas absorptance is very low. Here the physical control is internal leaf structures. The middle-infrared sector (1350-2500 nm) of the spectrum for vegetation is characterized by transition. As wavelength increases, both reflectance and transmittance generally decrease from medium to low. Absorptance, on the other hand, generally increases from low to high. Additionally, at three distinct places in this wavelength domain, strong water absorption bands can be observed. The primary physical control in these middle-infrared wavelengths for vegetation is *in vivo* water content. Internal leaf structure plays a secondary role in controlling energy-matter interactions at these wavelengths.

© 1999 David P. Lusch, Ph.D.

Solar Spectral Exitance 2.6

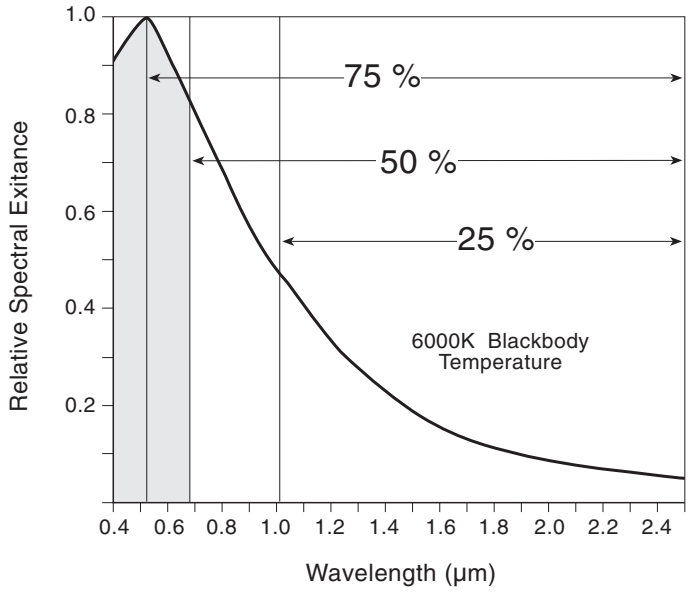

Spectral Partitioning by Vegetation 2.7

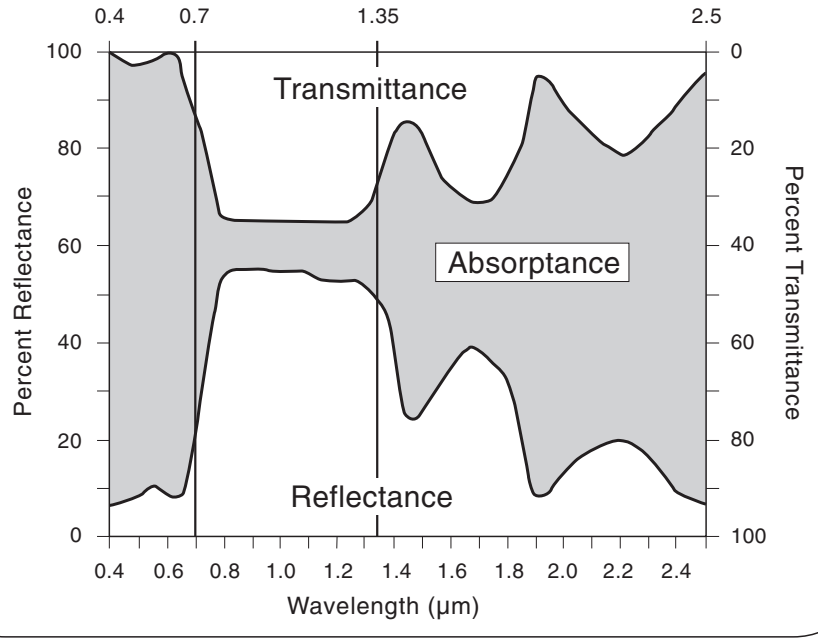

© 1999 David P. Lusch, Ph.D.

Visible Reflectance. The dominant plant pigments are the chlorophylls. These compounds exhibit pronounced absorptance of the bluish (400-500 nm) and reddish (600-700 nm) wavelengths (Figure 2.8.) This absorption of solar energy by vegetation is, of course, required in order to support photosynthesis. As noted above, transmittance by vegetation in the visible wavelengths is very low. Irradiance which has not been absorbed will be reflected. Thus, Chlorophyll-bearing vegetation appears green as a result of its minor reflectance peak in the 500-600 nm wavelengths.

There are other plant pigments, the carotenes and xanthophylls, which produce yellow or orange reflectances. Figure 2.9 shows the single, broad absorptance band, centered at about 450 nm, associated with these compounds. Although frequently present in green leaves, the solitary absorption feature produced by these pigments is usually masked by the chlorophyll absorptance. During stress or senescence, however, chlorophyll production usually declines and blue absorption (i.e. yellow reflectance) of the carotenes/xanthophylls may become obvious.

The anthocyanins are another type of plant pigment. They absorb the bluish and greenish wavelengths, giving rise to their red reflectance (Figure 2.9). These compounds are also frequently present in green foliage, but are masked by chlorophyll absorption. Some plant species (e.g. red maple *Acer rubrum*) produce large quantities of anthocyanin during autumn senescence at a time when chlorophyll production is declining. The resulting shift in spectral absorptance accounts for the bright red leaf color.

As plant senescence progresses, the changes in relative abundance of the various pigments are accompanied by shifts in spectral absorptance and reflectance. Figure 2.10 illustrates the temporally dynamic nature of visual foliar reflectance.

Near-Infrared Reflectance. Experiments by Moss (1951), Pearman (1966), Woolley (1971), Gausman (1977), and others have demonstrated that leaf reflectance occurs internally. The fundamental mechanism responsible for this phenomenon is the refractive index differences between the various internal leaf structures (cell walls, air spaces, chloroplasts, etc.). Leaves which were vacuum infiltrated with various liquids reflected less energy in the 400-2500 nm wavelengths than non-infiltrated leaves (Figure 2.11). Note that the near-infrared (NIR) reflectance was the most altered in these experiments, followed by the middle-infrared reflectance.

© 1999 David P. Lusch, Ph.D.

Chlorophyll Compounds 2.8

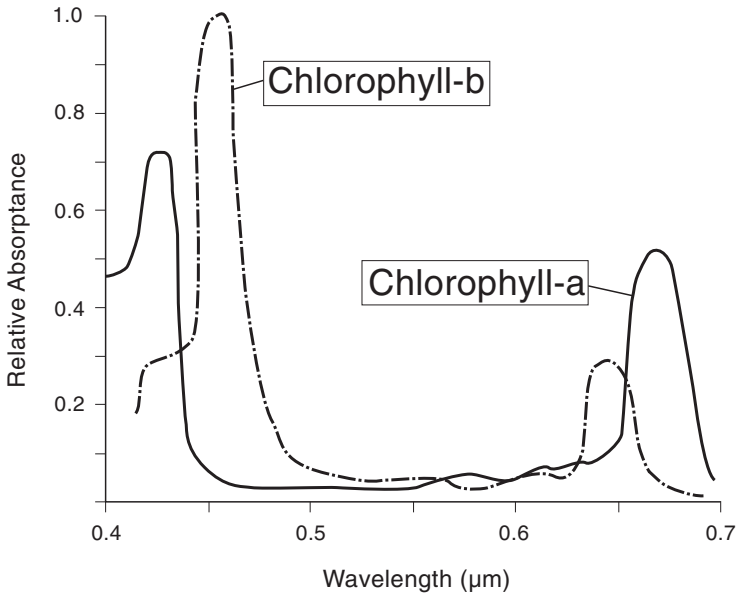

Non-green Pigments 2.9

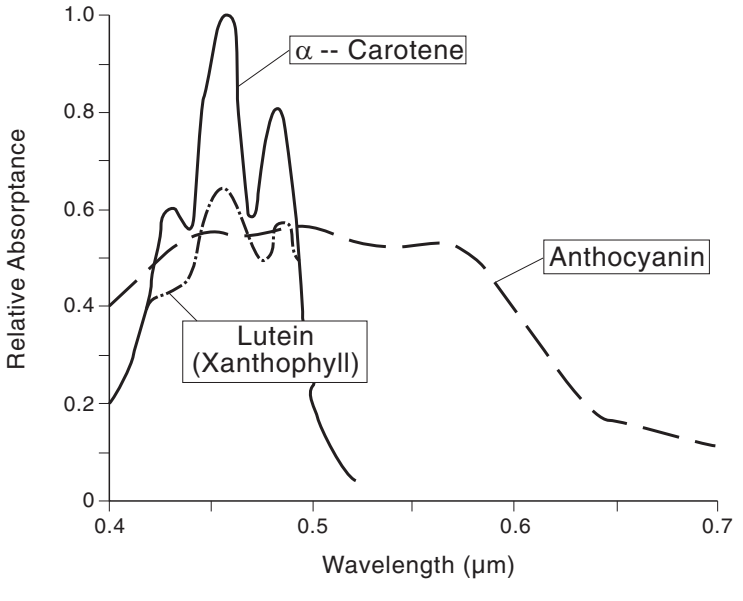

© 1999 David P. Lusch, Ph.D.

Senescence 2.10

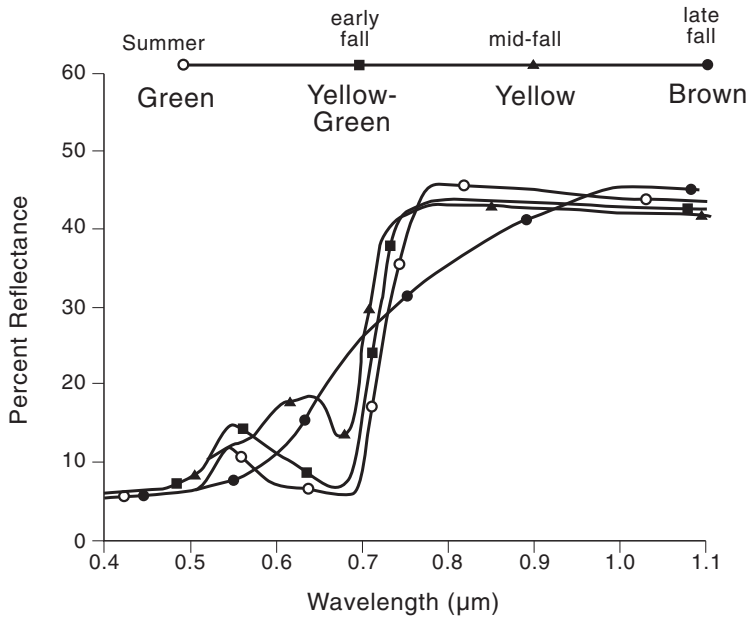

NIR Foliar Reflectance 2.11

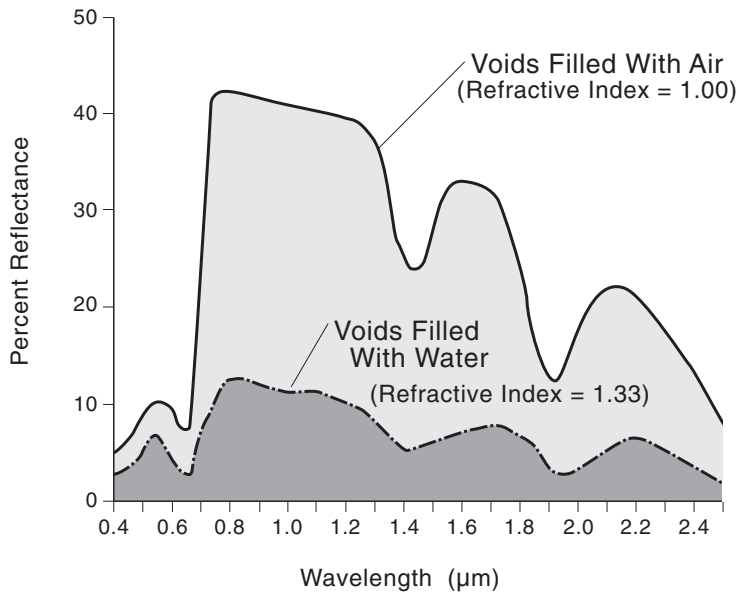

© 1999 David P. Lusch, Ph.D.

There are two common types of structural arrangements within leaves. The dorsiventral leaf structure, typical of dicots, has palisade mesophyll along the upper leaf side and spongy mesophyll composing the lower portion (Figure 2.12). The compact leaf structure typical of monocots, in contrast, presents a relatively densely-packed mesophyll lacking the long, prism-like palisade cells and containing very few large intercellular air voids. Internal leaf structure exerts little control on visible reflectance. In the infrared spectrum, dorsiventral leaves - containing numerous large air voids - reflect more long-wavelength radiation than compact leaves (Figure 2.13).

The important role these internal air voids play in controlling infrared reflectance is highlighted by observing leaf maturation. From a structural standpoint, dorsiventral leaves grow by pulling themselves apart internally (Figure 2.14). Immature dorsiventral leaves exhibit a compact, overall mesophyll arrangement. The lacunate mesophyll associated with older dorsiventral leaves contains many more air spaces. The relationships between spectral reflectance and leaf maturity are illustrated in Figure 2.15. Since young, immature leaves contain less chlorophyll and fewer air voids than older leaves, they reflect more visible light and less infrared radiation.

The most well-known near-IR reflectance difference between vegetation types is that which can be observed between broadleaf and needleleaf arboreal species. This very useful relationship, shown in Figure 2.16, exhibits indistinguishable spectral reflectances in the visible wavelengths, but easily recordable differences in the photographic infrared. Although stand conditions such as site index, age class, canopy closure, disturbance history, etc. will promote within-class differences, in general, broadleaf trees will reflect much more (> 10 % more) NIR radiation than needleleaf trees. These large differences in NIR reflectance are the result of several factors:

1. At the leaf level of observation, the broad leaves have a dorsiventral internal leaf structure while the needle leaves have a compact internal structure.

2. At the plant level of observation, most broadleaf trees have a much higher leaf-area / stem-branch-trunk area ratio compared to needleleaf trees. The non-foliar stems, branches and trunks tend to absorb NIR radiation.

3. At the canopy level of observation, most well-stocked broadleaf canopies present an upper reflectance surface that is nearly

c 1999 David P. Lusch, Ph.D.

Leaf Structures

2.12

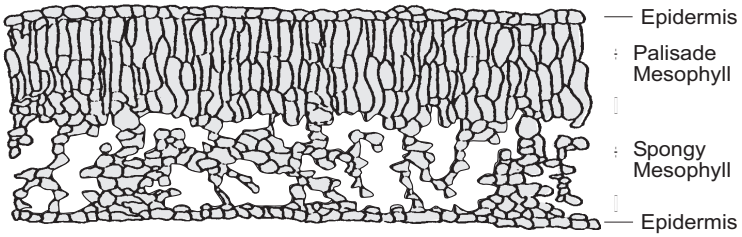

Dorsiventral Leaf Structure
(typical of dicots)

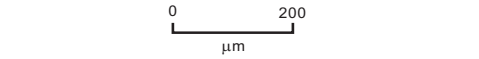

Compact Leaf Structure
(typical of monocots)

Effect of Leaf Structure on Reflectance

2.13

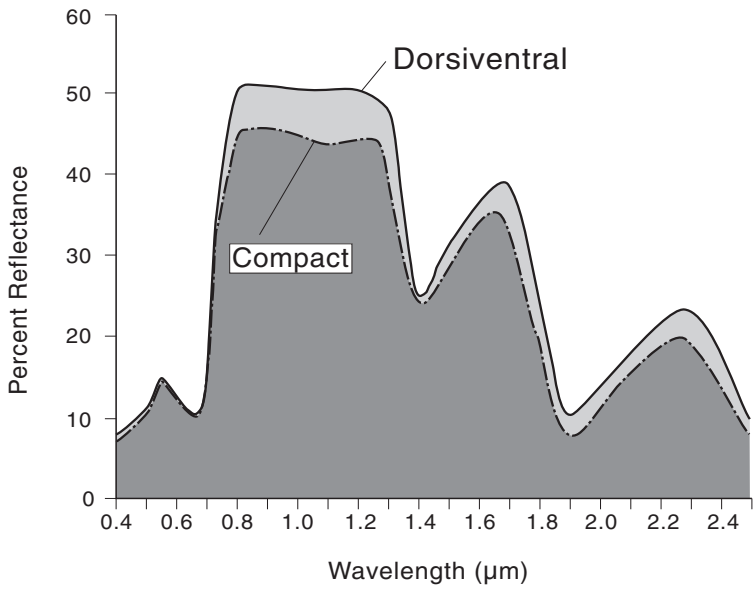

© 1999 David P. Lusch, Ph.D.

Dorsiventral Leaf Maturation

2.14

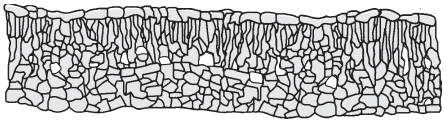

Young Leaf
Compact Mesophyll
(Few Air Spaces)

Older Leaf
Lacunate Mesophyll
(Many Air Spaces)

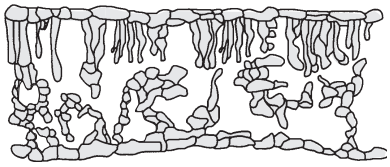

Leaf Maturity

2.15

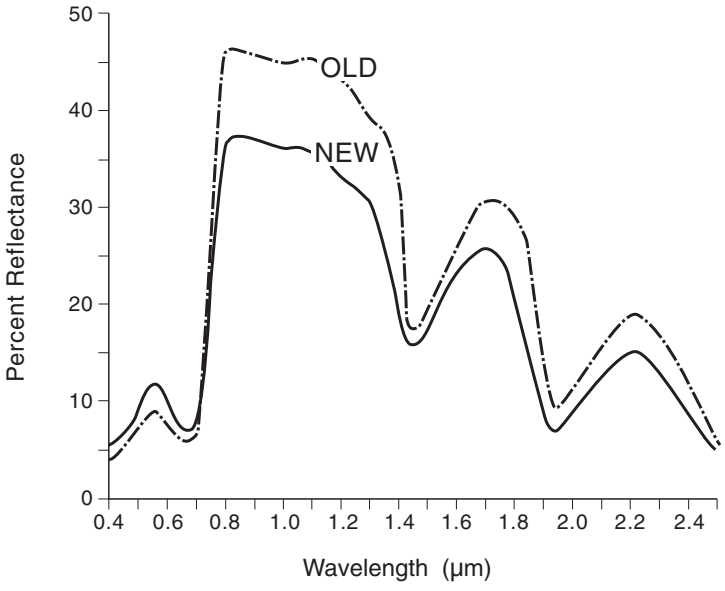

© 1999 David P. Lusch, PI

Spectral Signatures of Deciduous and Coniferous Trees

2.16

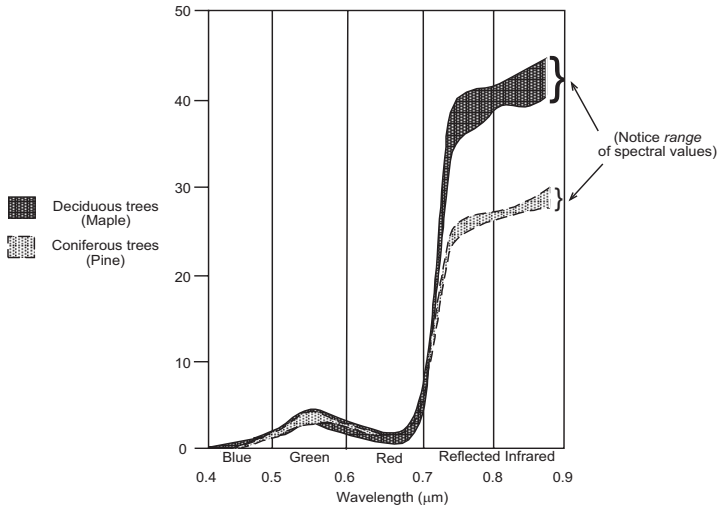

from: Kalensky, Z. and Wilson, D.A. 1975. Spectral Signatures of Forest Trees. Proc., Third Canadian Symposium on Remote Sensing. pp. 155-171

© 1999 David P. Lusch, Ph.D.

unbroken foliar material (i.e. high NIR reflectance) with fewer dark shadows compared to the needleleaf canopy which, even when well stocked, presents many inter-tree gaps and shadows. In large part, this is due to the differences in growth forms between the two types: broadleaf trees tend to have a rounded or bulbous form compared to the near conical form of needleleaf trees.

Foliar infrared reflectance is also altered by the number of leaf layers present in the canopy. In the near infrared especially, there is very little absorption - any irradiance that is not reflected will be transmitted. The impact of these energy-matter interactions can be illustrated using the overly-simplistic reflectance model shown in Figure 2.17. In this example, it is assumed that all of the irradiance is divided equally between reflectance and transmittance.

As a consequence of minimal absorptance in the near infrared, there is a limited, but useful, relationship between foliar biomass and NIR reflectance (Figure 2.18). As the number of leaf layers increases (increasing leaf area), infrared reflectance increases, especially in the NIR. Note that visible light reflectance remains unchanged since transmission is near zero. Note that beyond a certain point, called the infinite or asymptotic reflectance level, increasing leaf area has no impact on spectral reflectance.

One digital processing technique that seeks to take advantage of these reflectance relationships in the visible and NIR is called the **Normalized Difference Vegetation Index (NDVI)**. It uses image algebra and is defined as:

NIR - Red / NIR + Red

That is, the difference between the red light reflectance and the near infrared reflectance divided by their sum. The division by the sum of the red light and the NIR light is an attempt to normalize this index so that it may be used for multi-temporal or inter-scene comparison work. The premise of the index is that only vegetation, among the three major classes of earth cover types, possesses a large difference between its red light reflectance (due to chlorophyll absorption) and its NIR reflectance (due to high NIR transmissivity and, therefore, added NIR reflectance from deep within a vegetation canopy.

Numerous studies, using multispectral imagery of various spatial resolutions, have related NDVI values to canopy leaf area index (LAI). LAI is the amount of leaf surface area per unit ground area, and is widely used to describe the photosynthetic and transpirational surface of plant canopies. Using high-spatial-resolution data

c 1999 David P. Lusch, Ph.D.

NIR Reflectance Model

2.17

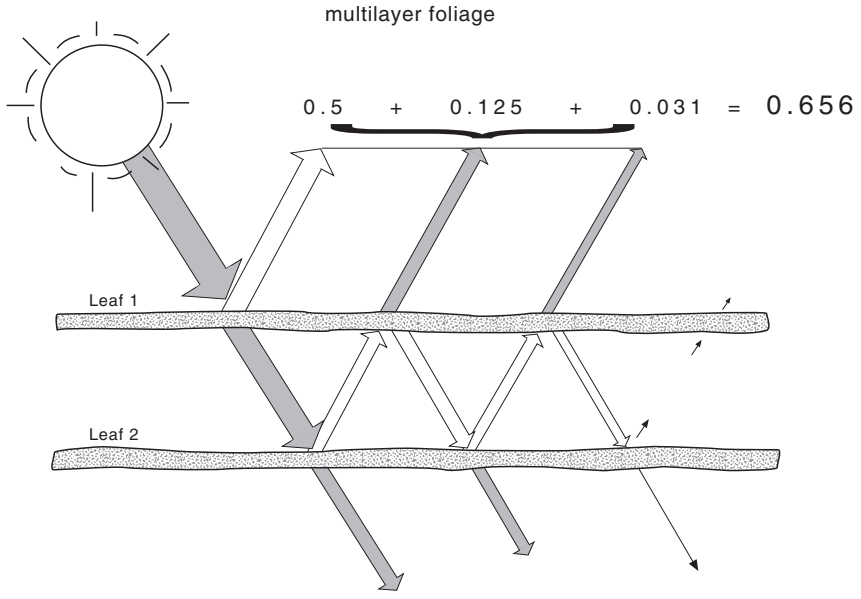

Leaf Area

2.18

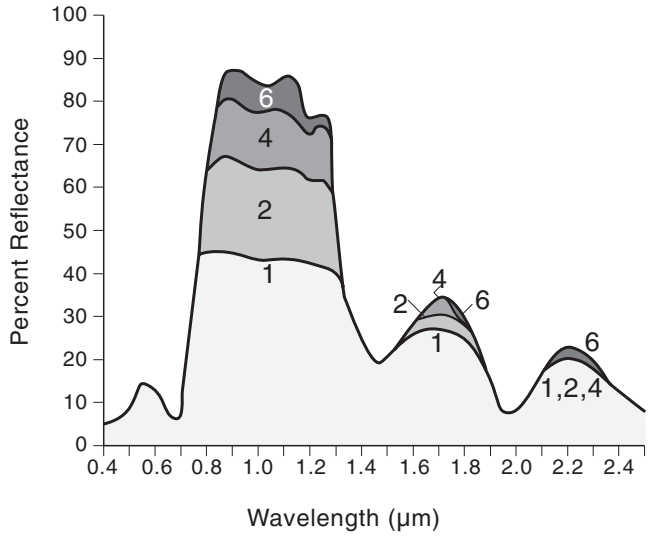

© 1999 David P. Lusch, Ph.D.

(pixels = 2.23 x 2.46 meters or 2.23 x 9.45) from the Compact Airborne Spectrographic Imager (CASI), Gong *et al.* (1995) demonstrated a very strong statistical relationship (r^2=0.971, rmse = 0.764) between measured-LAI and predicted-LAI (Figure 2.19). In the best case, they used NDVI values calculated from a NIR band at 761.4 - 770.2 nm and a red-light band at 601.0 - 609.8 nm. Other bands on the CASI instrument yielded somewhat lower r-squared values in relating the NDVI value to the measured LAI value (r^2 = 0.970, rmse = 0.848 and r^2 = 0.968, rmse = 1.151). Importantly, these investigators mention that, "NDVI starts to saturate before LAI reaches 6." The western montane forest canopies they were studying had LAI values that peaked between 8 and 13.

Using Thematic Mapper Simulator data (24 x 24 meter pixels), Peterson *et al.* (1987) also reported a very strong statistical relationship between measured LAI and the NIR / red ratio. This study also used montane forest canopies as its target that had LAIs that varied from 1 to 16. As shown in Figure 2.20, a log-linear relationship between the NIR/Red ratio and the measured leaf area index explained 91% of the variance (r^2 =0.91, S.E. = 0.77). These researchers also noted that, "The LAI to Near IR/red relationship slowly became asymptotic, reaching a saturation level at about an LAI of ten."

Even at the coarse spatial resolution of the AVHRR instrument (pixels = 1.2 km2), Spanner *et al.* (1990) reported reasonably strong statistical relationships between measured LAIs of montane forest canopies and the NDVI (Figure 2.21). In their best fit from July 1987, the r^2 =0.789 with a standard error of 0.044. These results were obtained with monthly-maximum-NDVI composite imagery, so the lower explanation of variance is not unexpected. These authors noted, "...penetration of light into the forest canopy becomes asymptotic above an LAI of 5-6, so that some asymptotic behavior should be inherent in the relationship at an LAI above 6."

Middle-Infrared Reflectance. In the middle-infrared (MIR) wavelengths, leaf reflectance is inversely related to *in vivo* water content (Figure 2.22). Overall reflectance increases as a leaf desiccates. The rise in middle-infrared reflectance, compared to the shorter wavelengths sectors, is the most substantial. Within the MIR wavelengths, the greatest reflectance changes occur in the major water absorption bands at 1.45, 1.92, and 2.7 micrometers. The minor water absorption bands at 0.96 and 1.2 micrometers become notable spectral features in the reflectance curves of multi-layer

© 1999 David P. Lusch, Ph.D.

NDVI vs. LAI
High Spatial Resolution

2.19

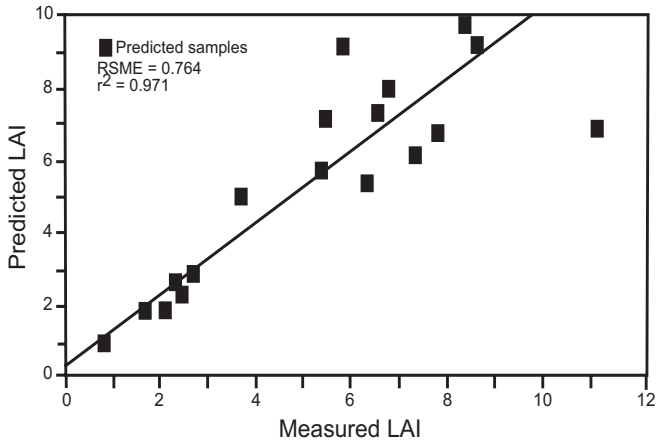

Predicted LAI derived from NDVI where NIR = 761.4 - 770.2 nm and Red = 601.0 - 609.8 nm

VI vs. LAI
Moderate Spatial Resolution

2.20

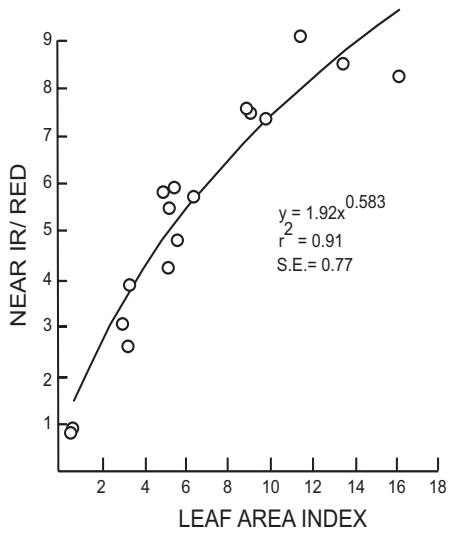

Relationship between the atmospherically corrected near IR/Red ratio and the LAI of the forest stands

© 1999 David P. Lusch, Ph.D.

NDVI vs. LAI
Coarse Spatial Resolution

2.21

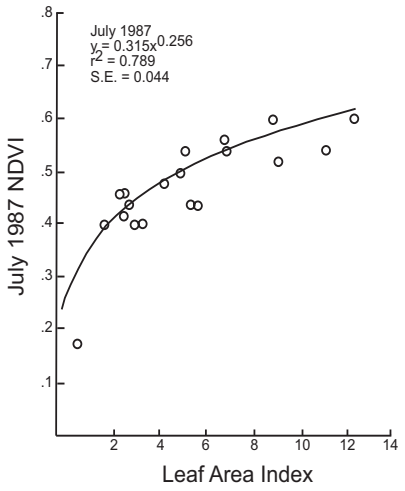

Relationship between leaf area index of the primary sites
and the monthly maximum value composite NDVI for July 1987

Leaf Moisture Content

2.22

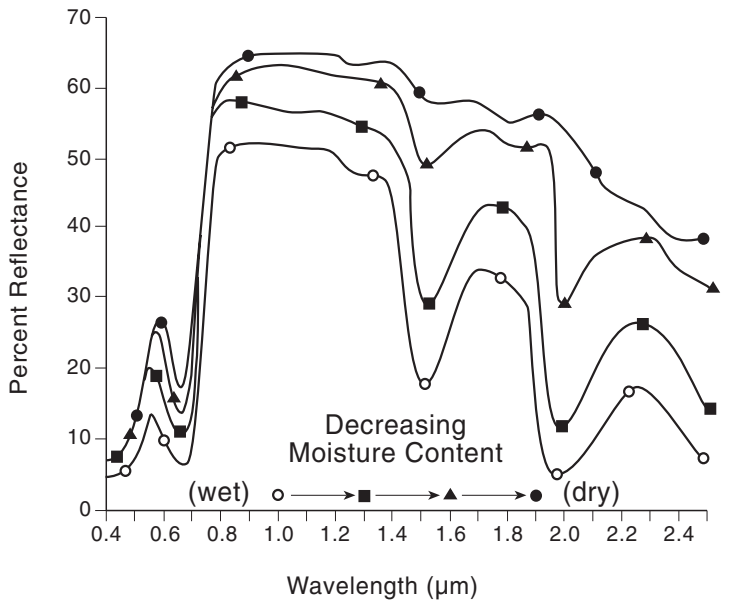

© 1999 David P. Lusch, Ph.D.

canopies. Note that long-path length remote sensing of middle-infrared radiation must be accomplished in the appropriate "atmospheric windows" - 1.5 to 1.8 and 2.0 to 2.6 micrometers - in between the major water absorption bands (Figure 2.23).

BioPhysical Controls of Soil Reflectance

The spectral reflectance of soil is controlled, for the most part, by six variables: moisture content, organic matter content, particle size distribution, iron oxide content, soil mineralogy, and soil structure (Obukhov and Orlov, 1964; Bowers and Hanks, 1965; Shields *et al*., 1968; Baumgardner *et al*., 1970; Bowers and Smith, 1972; Peterson *et al*., 1979; Stoner and Baumgardner, 1980, 1981). Of these variables, moisture content and organic matter are the most important (Figure 2.24)

Moisture Content. The near-surface moisture content of soil is the most important reflectance factor due to its dynamic nature and large overall impact on soil reflectance. As shown in Figure 2.25, there is an inverse relationship between edaphic moisture content and soil spectral reflectance. Note the persistence of the water absorption bands (1.45 and 1.92 micrometers) even in the air-dried sample. This results from water films being held tightly onto the relatively large proportion of very fine silt and clay particles in this particular soil. Also notable is the strong hydroxyl absorption band at 2200 nm which many clay-rich soils will exhibit. Comparing soils from different natural drainage classes, the better drained soils are more reflective (Figure 2.26).

Organic Matter Content. Mineral soils, as distinct from organic soils, are dominantly mineral material with less than 20 percent organic carbon by weight. As shown in Figure 2.27, for mineral soils, as the organic matter content increases, soil reflectance decreases. As shown in Figure 2.28, some researchers have demonstrated a workable relationship between remotely sensed soil reflectance and organic carbon content. The reflectance of organic soils, on the other hand, is controlled primarily by state of decomposition of the plant material (Figure 2.29). Peat (fibric material) is composed of plant remains which have undergone only minimal decomposition. This type of organic soil is usually dark brown to reddish-brown. The highly decomposed sapric material (muck) is generally black. Organic soils of intermediate decomposition are classed as hemic soils.

© 1999 David P. Lusch, Ph.D.

Atmospheric Transmissivity

2.23

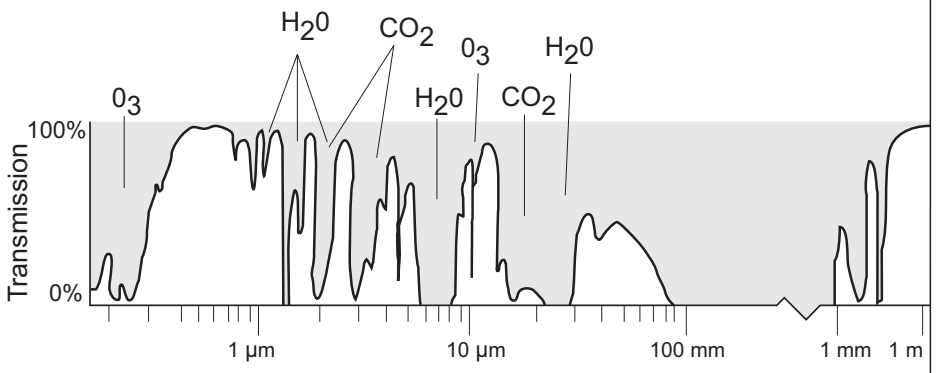

Soil Reflectance

2.24

Six Controlling Factors

Most Important Factors

1. Moisture Content
2. Organic Matter Content

Other Factors

3. Particle Size (surface)
4. Iron Oxide Content
5. Mineralogy
6. Structure

© 1999 David P. Lusch, Ph.D.

Soil Moisture Content

2.25

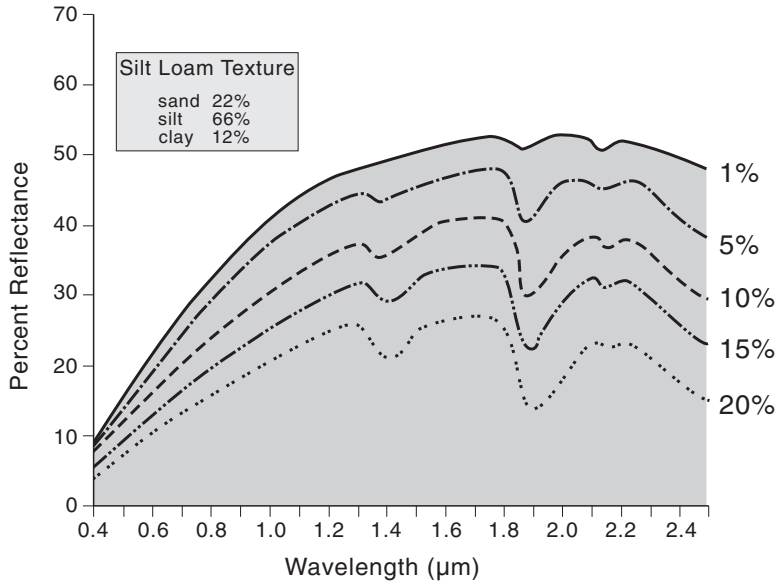

Soil Drainage

2.26

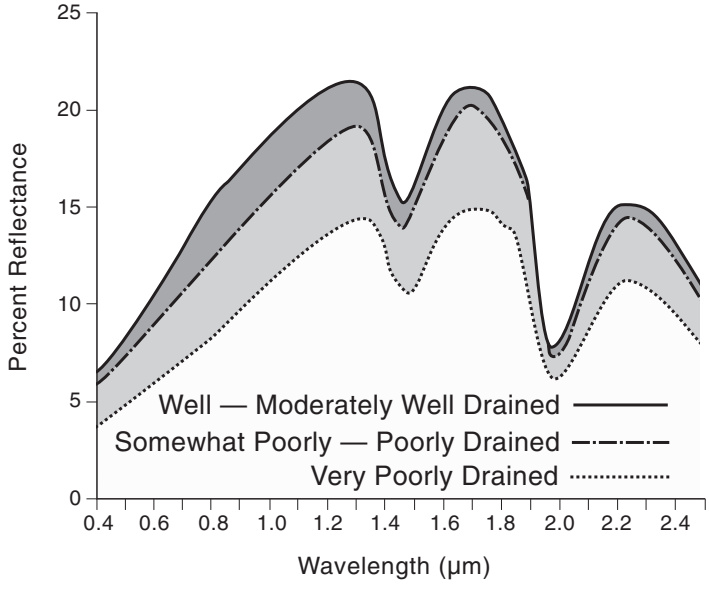

© 1999 David P. Lusch, Ph.D.

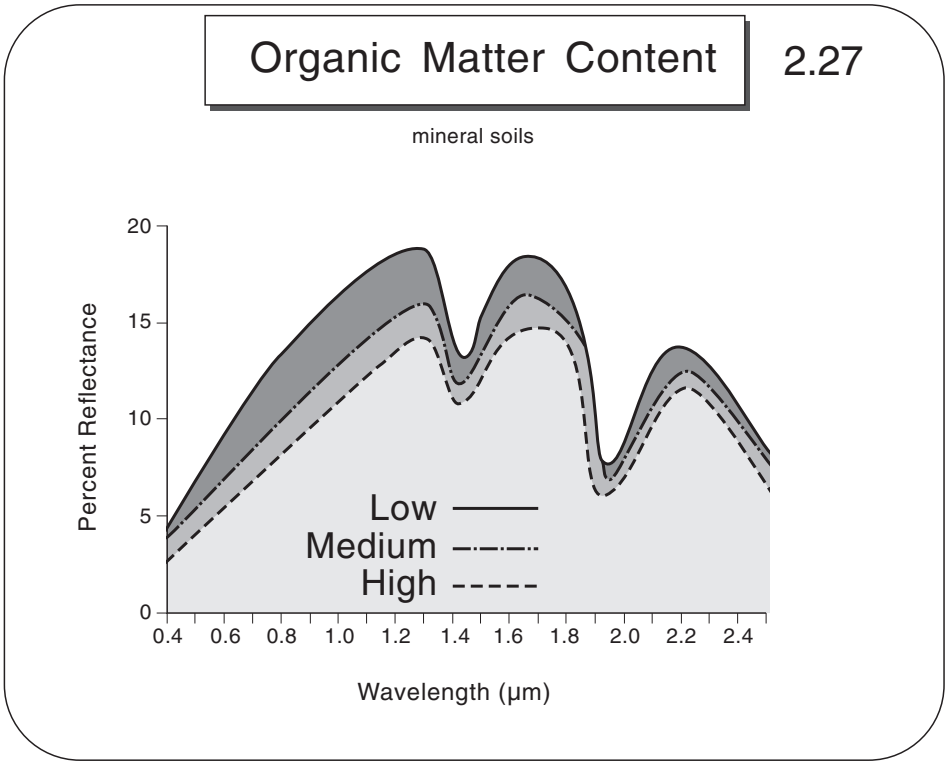

c 1999 David P. Lusch

Relationship between soil organic carbon and Landsat TM data in eastern Washington

2.28

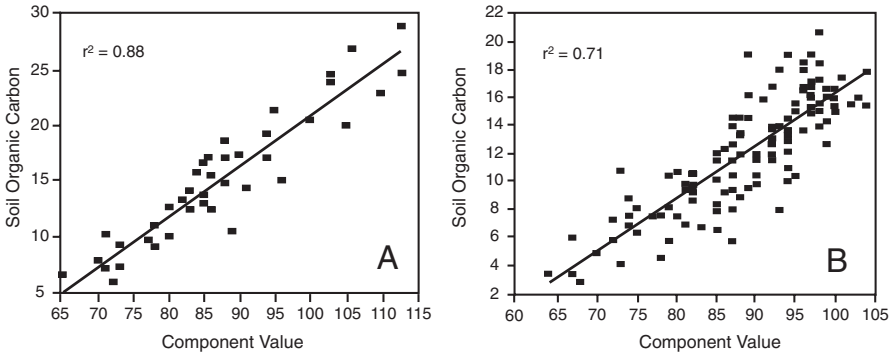

Regression function comparing the association between measured s.o.c. content and observed Landsat TM values for the pooled Plaza and Pullman, Washington field sites (A) and the pooled Thera and St. John, Washington field sites.

Wilcox, Cindy H., Frazier, Bruce E., and Ball, Shane T.1994. **Relationship between Soil Organic Carbon and Landsat TM Data in Eastern Washington.** Photogrammetric Engineering and Remote Sensing. Vol 60, No. 6 (June), pp. 777-781.

Processing notes:

2 pixel by 2 pixel spatial average (28.5m x 2 = 57m)

Atmospheric correction performed (Chavez's dark object subtraction)

DN's converted to Radiances

Ratios: 1/4; 3/4; 5/4; 5/3

PC Transformation: PC1: greeness variation
PC2: soils variation
PC3: wetness variation

Regressed PC2 vs Soil Organic Carbon of pooled samples

© 1999 David P. Lusch, Ph.D.

Organic Soils

2.29

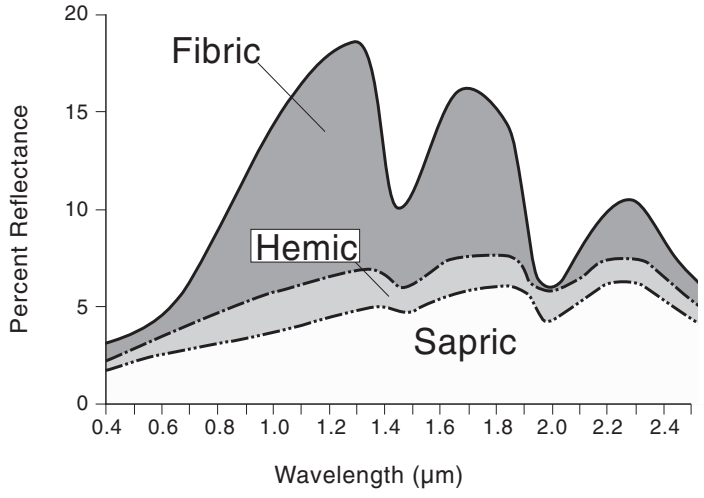

© 1999 David P. Lusch, Ph.D.

Particle Size Distribution. The larger-diameter particle sizes (e.g. medium sand, coarse sand, etc.) exhibit pronounced interstitial voids. This increased surficial micro-roughness, compared to the fine particle sizes, presents many more "light traps" to any irradiance. Assuming the other soil factors are equal, the finer particle sizes will exhibit greater soil reflectances (Figure 2.30). With moisture content equilibrated, and the organic matter content naturally similar, the multi-sample data presented in Figure 2.31 illustrate the relationship between soil texture and spectral reflectance.

Iron Oxide Content. Iron oxide (Fe_2O_3) is one of the primary causes of the red colors in many soils. Iron oxide content and organic matter content are the two most important soil properties affecting the spectral reflectance characteristics of eroded soils, particularly in the 500 to 1200 nm region (Weismeiier *et al*., 1984). The data presented in Figure 2.32 illustrate the relationship between iron oxide content and soil spectral reflectance. Chemically removing the extractable iron oxides from a soil sample results in increased reflectance especially at wavelengths less than 1100 nm. A broad absorption feature, centered at 900 nm and attributed to iron oxide, is obvious in this graph.

BioPhysical Controls of Water Reflectance

Energy Partitioning. There are three types of possible reflectance from a water body - surface (specular) reflectance, bottom reflectance, and volume reflectance (Figure 2.33). Of these, only volume reflectance contains information relating to water quality. For deep (>2 m), clear water bodies, volume reflectance is very low (6-8 percent) and is confined to the visible wavelengths (Figure 2.34). Transmittance in these cases is very high especially in the blue-green part of the spectrum, but diminishes rapidly in the near-infrared wavelengths. Absorptance, on the other hand, is notably low in the shorter visible wavelengths, but increases abruptly in the near-infrared sector. Shallow water (<2 m deep) transmits significant amounts of NIR radiation (Figure 2.35). As depth increases, the peak transmittance wavelength for clear water decreases and finally stabilizes at about 480 nm.

Volume Reflectance. Clear water reflects very little solar irradiance, but turbid water is capable of reflecting significant amounts of sunlight (Figure 2.36). It is notable that the peak-reflectance point shifts to longer wavelengths as turbidity increases (Figure 2.37). As shown in Figures 2.38 and 2.39, as the chlorophyll content of a water body increases (resulting from an increase in algae, phytoplankton, etc.) its

© 1999 David P. Lusch, Ph.D.

Soil Particle Size 2.30

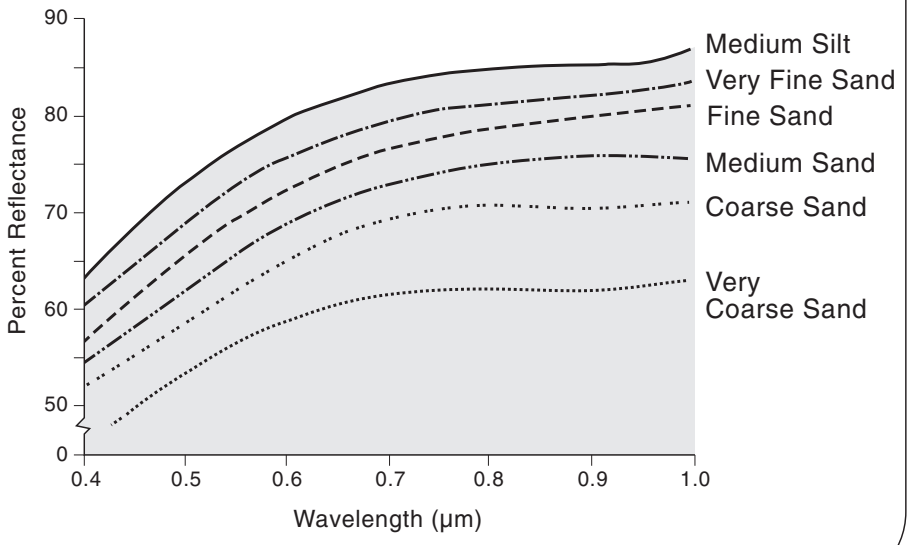

Soil Texture 2.31

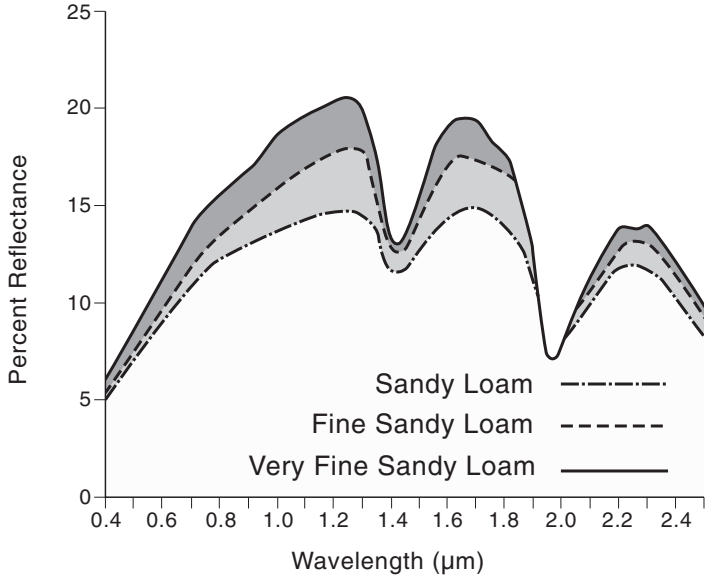

© 1999 David P. Lusch, Ph.D.

Iron Oxide in Soil

2.32

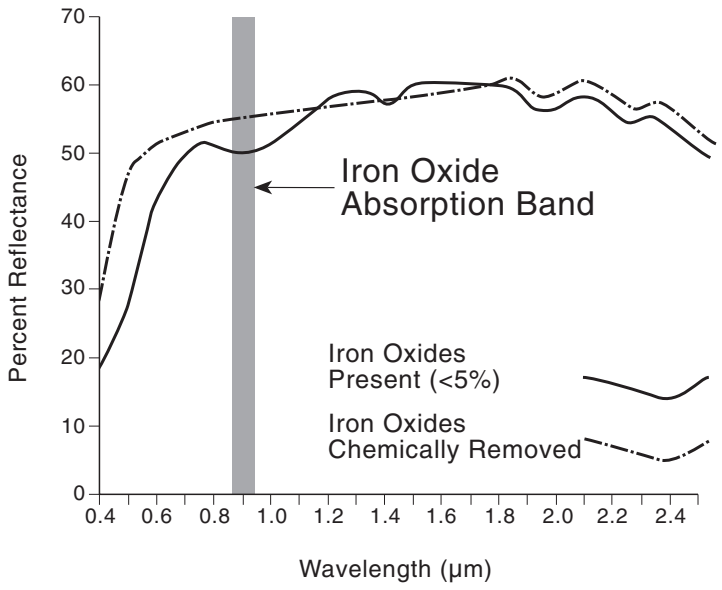

Water Reflectance

2.33

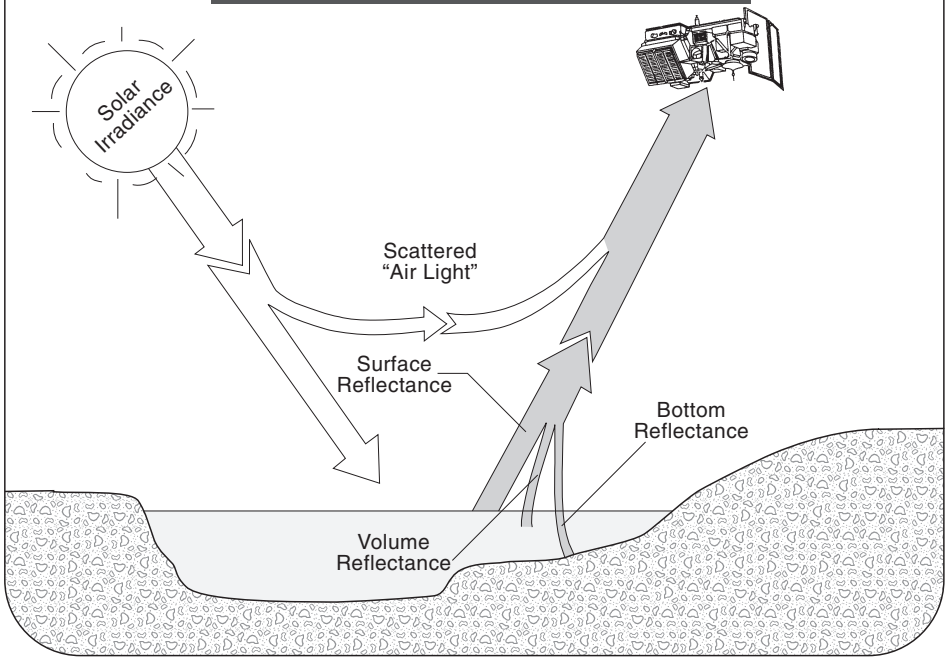

© 1999 David P. Lusch, Ph.D.

Spectral Partitioning by Water

2.34

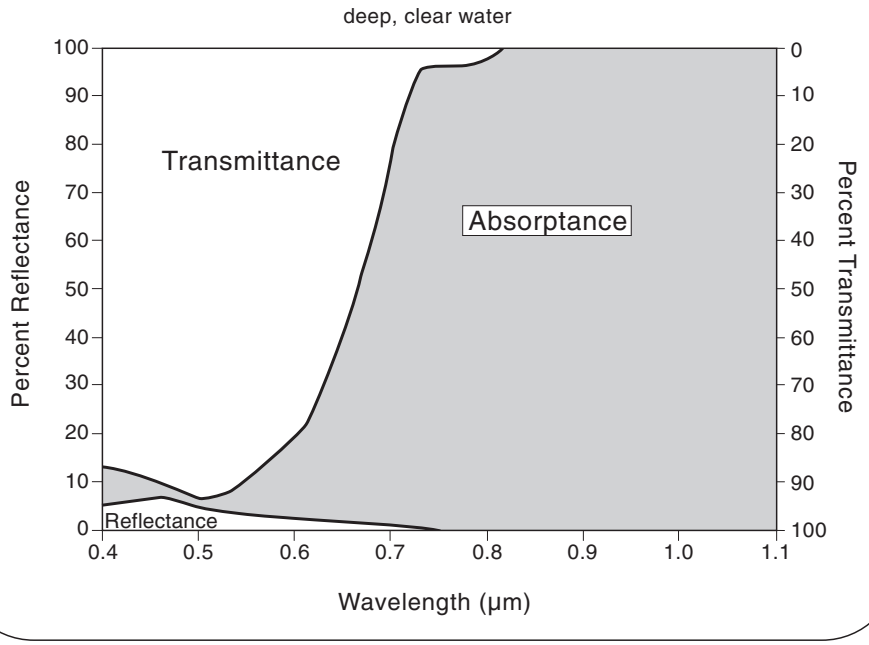

Water Transmittance

2.35

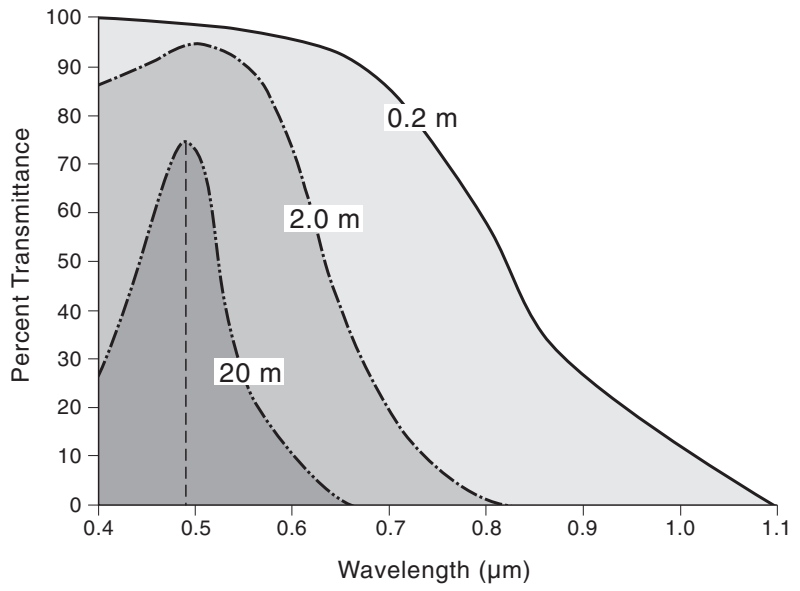

© 1999 David P. Lusch, Ph.D.

Water Turbidity

2.36

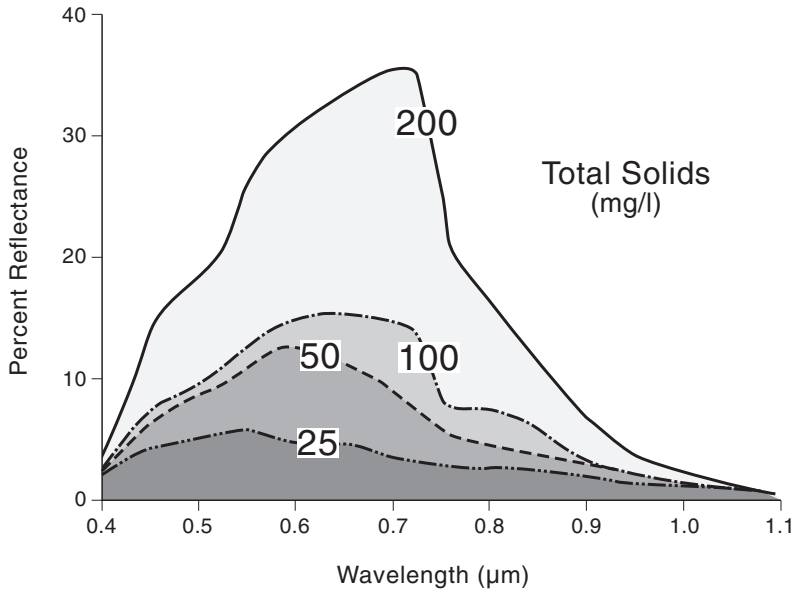

Water Turbidity

2.37

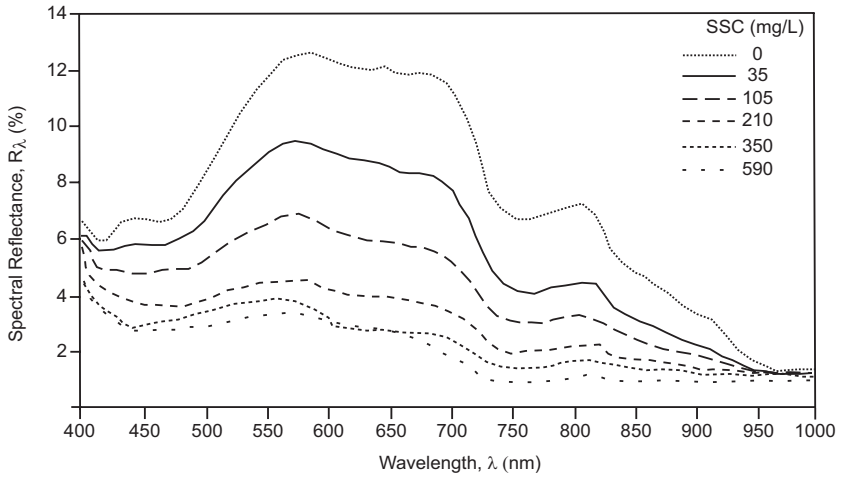

Chen, Z. P.J. Curran, and J.D. Hansom. 1992. Derivative Reflectance Spectroscopy to Estimate Suspended Sediment Concentration. Remote Sensing of Environment, v. 40, pp. 67-77.

© 1999 David P. Lusch, Ph.D.

Chlorophyll in Water

2.38

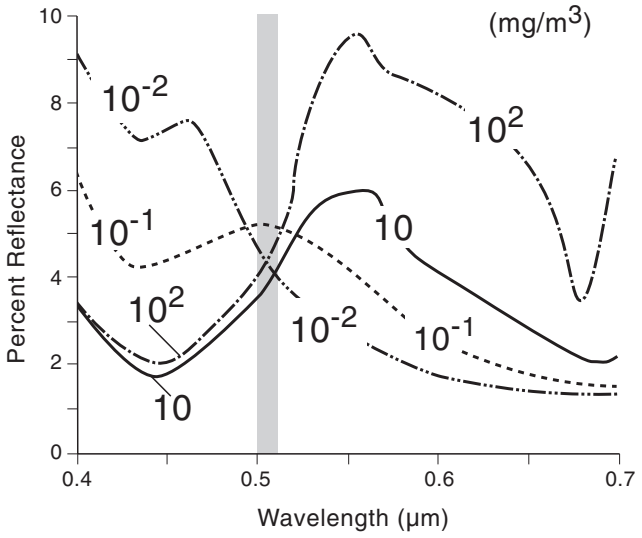

Chlorophyll in Fresh Water

2.39

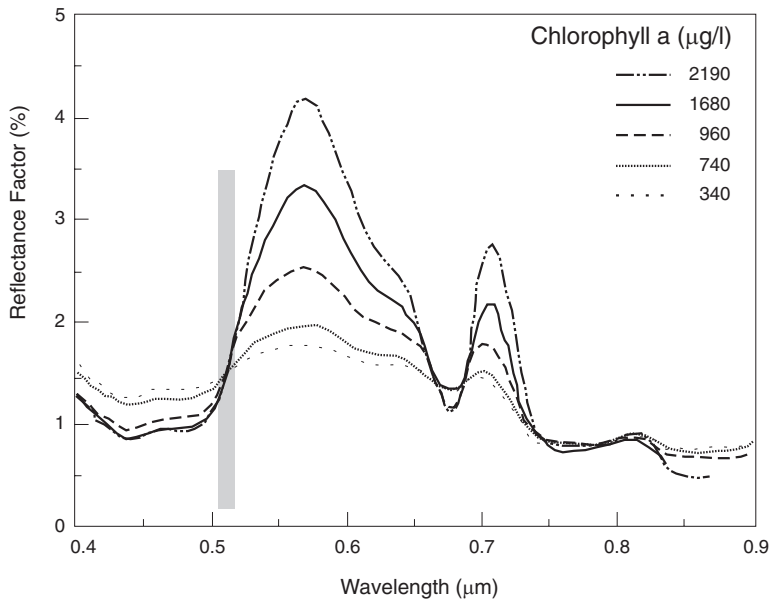

© 1999 David P. Lusch, Ph.D.

blue-light reflectance decreases while its green-light reflectance increases. The "hinge point" in this relationship, over four orders of magnitude of concentration differences, remains relatively stable at 510-520 nm. Also noteworthy, is the asymptotic reflectance change in the blue wavelengths as chlorophyll concentration increases compared to the reflectance differences in the longer wavelengths.

Clouds and Snow. Snow and clouds can be easily differentiated only in the middle-infrared portion of the spectrum (Figure 2.40). Snow reflectance is unique. It is very high in the visible and NIR wavelengths, but plummets to near zero in the water absorption bands, and remains at relatively low levels between them. In contrast, most clouds act as non-selective scatterers and reflect significant amounts of solar irradiance across the 400-2500 nm spectrum.

Summary

The reflectance, absorptance, and transmittance characteristics of generalized vegetation, soil, and water features have been summarized using graphical examples from the research literature. This synthesis is designed to facilitate our understanding of the principal, physical controls of these energy-matter interactions. These relationships are assumed to be fundamental to fully comprehending any remotely-sensed data acquired in the 400-2500 nm spectrum.

© 1999 David P. Lusch, Ph.D.

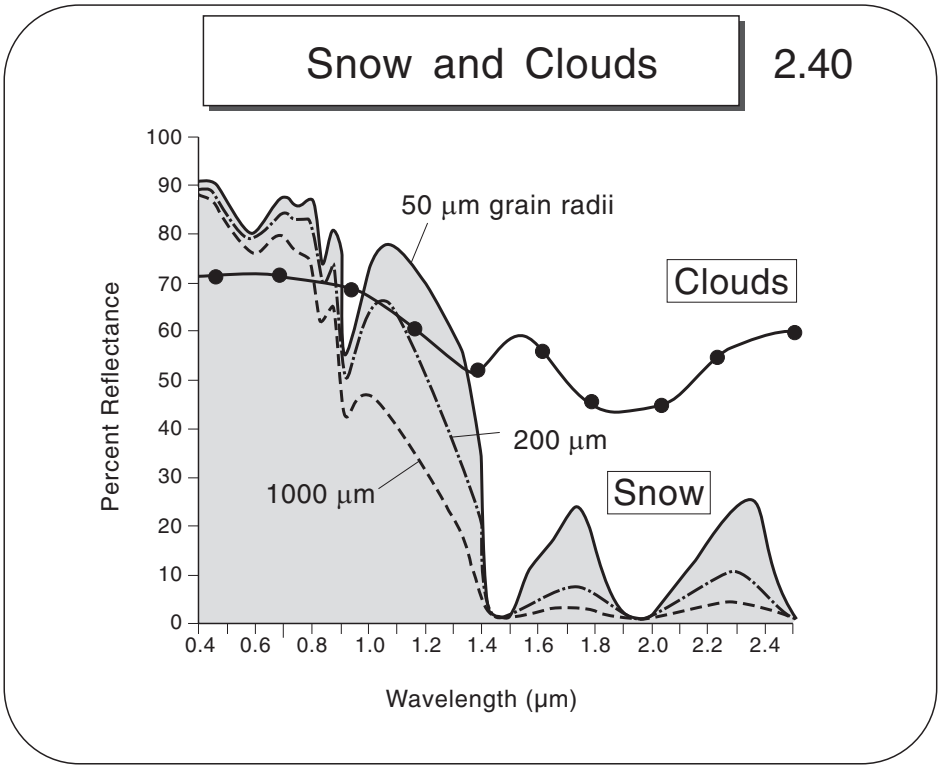

© 1999 David P. Lusch, Ph.D.

References

Baumgardner, M.F., S.J. Kristof, D.J. Johannsen, and A.L. Zachary. 1970. Effect of organic matter on the multi-spectral properties of soils. *Proceedings, Indiana Academy of Sciences.* 79: 413-422.

Bowers, S.A. and R.J. Hanks. 1965. Reflection of radiant energy from soils. *Soil Science.* 100: 130-138.

Bowers, S.A. and S.J. Smith. 1972. Spectrophotometric determination of soil water content. *Soil Science Society America Proceedings.* 36: 978-980.

Bowker, D.E., R.E. Davis, D.L. Myrick, K. Stacy, and W.T. Jones. 1985. *Spectral Reflectances of Natural Targets for Use in Remote Sensing Studies.* NASA Reference Pub. 1139. 181 p.

Curan, P.J. 1985. *Principles of Remote Sensing.* NY: Longman. 282 p.

Dozier, J. 1984. Snow reflectance from Landsat-4 Thematic Mapper. *In* J. Barker, ed. *Landsat-4 Science Investigations Summary.* NASA Conference Pub. 2326. 142-147.

Gates, D.M. 1980. *Biophysical Ecology.* N.Y.: Springer-Verlag. 611 p.

Gausman, H.W. 1977. Reflectance of leaf components. *Remote Sensing of Environment.* 6: 1-9.

Gausman, H.W. 1985. *Plant Leaf Optical Properties in Visible and Near-Infrared Light.* Graduate Studies No. 29. Lub bock, Texas: Texas Tech Press. 78 p.

Gong, P., R. Pu, and J.R. Miller. 1995. Coniferous Forest Leaf Area Index Estimation Along the Oregon Transect Using Compact Airborne Spectrographic Imager Data. PE & RS, v. 61, n.9 (Sept), pp. 1107-1117

Hoffer, R.M. 1978. Biological and physical consideration in applying computer-aided analysis techniques to remote sensor data. *In* P.H. Swain and S.M. Davis, eds. *Remote Sensing: The Quan titative Approach.* NY: McGraw-Hill. 227-289.

Hoffer, R.M. and C.J. Johannsen. 1969. Ecological potentials in spectral signature analysis. *In* P.L. Johnson, ed. *Remote Sensing in Ecology.* Athens, Georgia: University of Georgia Press. 1-16.

Karmanov, I.I. 1970. Study of soils from the spectral composition of reflected radiation. *Soviet Soil Science.* 4: 226-238.

Mathews, H.L., R.L. Cunningham, and G.W. Petersen. 1973. Spectral reflectance of selected Pennsylvania soils. *Soil Science Society America Proceedings.* 37: 421-424.

Milton, E.J. 1987. Principles of field spectroscopy. *Internaional Journal Remote Sensing.* 8: 1807-1827.

© 1999 David P. Lusch, Ph.D.

Moore, G.K. 1978. Satellite surveillance of physical water-quality characteristics. *Proceedings Twelfth International Symposium Remote Sensing Environment.* Ann Arbor, Michigan: Environmental Research Institute of Michigan. 445-462.

Moss, R.A. 1951. *Absorption Spectra of Leaves.* Ph.D. Thesis. Ames, Iowa: Iowa Sate University. 68 p.

Myers, V.I. 1970. Soil, water and plant relations. *In* Committee on Remote Sensing for Agricultural Purposes, National Research Council, eds. *Remote Sensing with Special Reference to Agriculture and Forestry.* Washington, D.C.: National Academy of Sciences. 253-297.

Obujov, A.I. and D.S. Orlov. 1964. Spectral reflectivity of the major soil groups and possibility of using diffuse reflection in soil investigations. *Soviet Soil Science.* 2: 174-184.

Pearman, G.I. 1966. The reflection of visible radiation from leaves of some western Australian species. *Australian Journal Biological Science.* 19: 97-103.

Peterson D.L., M.A. Skinner, S.W. Running, and K.B. Teuber. 1987. Relationship of Thematic Mapper Simulator Data to Leaf Area Index of Temperate Coniferous Forests. Remote Sensing of Environment. v. 22, pp. 323-341.

Peterson, J.B., B.F. Robinson, and R.H. Beck. 1979. Predictability of change in soil reflectance on wetting. *Proceedings Symposium Machine Processing of Remotely Sensed Data.* West Lafayette, Indiana: Purdue University. 264-274.

Ritchie, J.C., J.R. McHenry, F.R. Schiebe, and R.B. Wilson. 1974. The relationship of reflected solar radiation and the concentration of sediment in surface reservoirs. *In* F. Shahrokhi, ed. *Remote Sensing of Earth Resources, v. III.* Tullahoma, Tennessee: University of Tennessee Space Institute. 57-72.

Shields, J.A., E.A. Paul, R.J. St. Amaud, and W.K. Head. 1968. Spectrophotometric measurement of soil color and its relationship to moisture and organic matter. *Canadian Journal Soil Science.* 48: 271-280.

Spanner, M.A., L.L. Pierce, S.W. Running and D.L. Peterson. 1990. The seasonality of AVHRR Data of Temperate Coniferous Forests: Relationship with Leaf Area Index. Remote Sensing of Environment. v. 33, pp. 97-112.

Stoner, E.R. and M.F. Baumgardner. 1980. *Physicochemical, site, and bidirectional reflectance factor characteristics of uniformly moist soils.* LARS Technical Report 111679. West Lafayette, Indiana: Laboratory for Applications of Remote Sensing, Purdue University. 94 p.

© 1999 David P. Lusch, Ph.D.

Stoner, E.R. and M.F. Baumgardner. 1981. Characteristic variations in reflectance of surface soils. *Soil Science Society America Journal*. 45: 1161-1165.

Weismiller, R.A., G.E. Van Scoyc, S.E. Pazar, K. Latz, and M.F. Baumgardner. 1984. Utilization of spectral properties of soils for monitoring soil erosion. *Proceedings International Congress Soil Erosion and Conservaion.* Honolulu, Hawaii.

Wolfe, W.L. and G.J. Zissis, eds. 1978. *The Infrared Handbook.* Washington, D.C.: Office of Naval Research, Dept. of the Navy. 1709 p.

Woolley, J.T. 1971. Reflectance and transmittance of light by leaves. *Plant Physiology.* 47: 656-662.

Reference for Figure 2.39

Rundquist, D.C., L. Han, J.F. Schalles and J.S. Peake. 1996. Remote measurement of algal chlorophyll in surface waters: the case for the first derivative of reflectance near 690 nm. Photogrammetric Engineering & Remote Sensing. 62:195-200.

© 1999 David P. Lusch, Ph.D.

c 1999 David P. Lusch, Ph.D.

Chapter 3	Videography

Contents

© 1999 David P. Lusch, Ph.D.

3.1 Objectives

- Compare the spatial and spectral resolution of video technology with film-based systems
- List four advantages and two disadvantages of video remote sensing
- Describe two applications which could benefit from the use of airborne videography

3.2 Introduction

Video is a Latin word meaning *I see.* Most of us are familiar with audio, meaning *I hear*, systems in which the microphone converts sound waves into electrical signals. In a video system, the sensor (either a vidicon tube or a solid state array) in the camera converts light energy into electrical signals. The sensor is to a video system what the microphone is to an audio system. The raw video signal is a fluctuating DC voltage. Bright objects in the scene are represented by higher voltages; dark parts of the scene are represented by lower voltages.

Just as an audio signal can be recorded on tape, so to the video signal can be tape recorded. However, recording video signals is a more difficult task because of the much higher frequencies associated with video data. High-fidelity sound recording, for instance, captures a frequency range of about 20 to 20,000 Hz. In marked contrast, the frequency range of video extends to 4 MHz or more — 200 times the range of audio!

3.3 Video Signal Recording

The amplitude-modulated, DC-voltage video signal is converted into a frequency-modulated signal by the video cassette recorder (VCR). As illustrated in Figure 3.1, the FM circuit in the VCR uses a voltage-controlled oscillator (VCO) for this purpose. The voltage fluctuations of the incoming video signal causes the oscillator's vibrational frequency to vary. For a VHS recording system, for example, the sync tip of the input video signal is locked at the voltage level which produces a 3.4 MHz oscillator output frequency. The video voltage associated with peak white, on the other hand, causes the oscillator frequency to increase to 4.4 MHz; this provides a total bandwidth of 1.0 MHz.

In North America, the format of video images is specified by the RS-170A standard from the National Television Standards Committee (NTSC). This requirement specifies that each

© 1999 David P. Lusch, Ph.D.

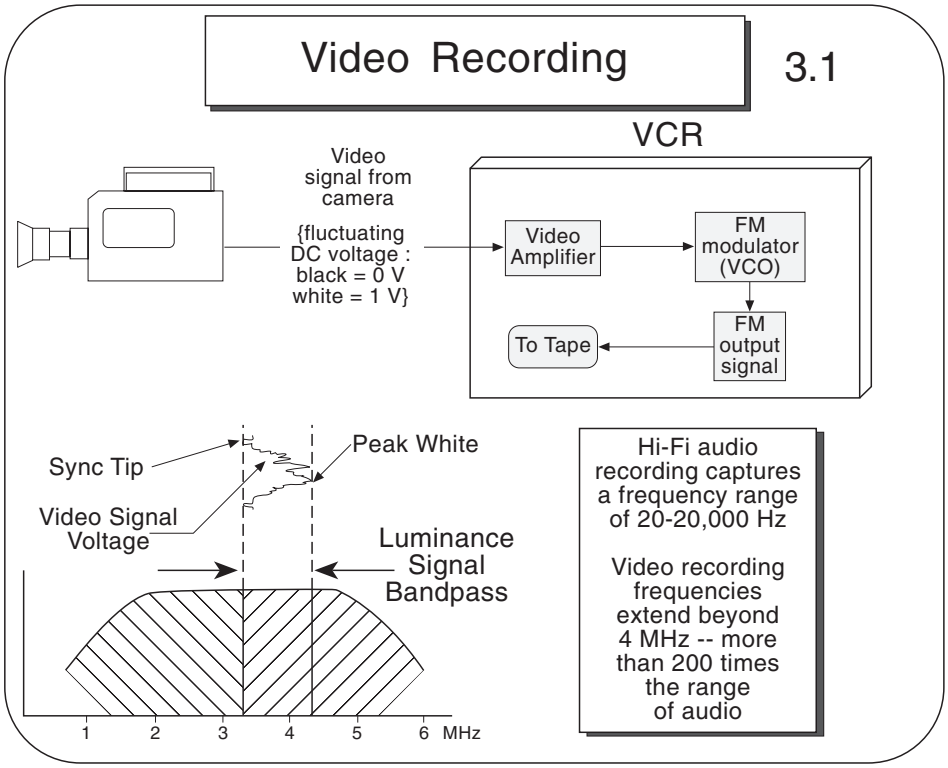

© 1999 David P. Lusch, Ph.D.

video picture (called a frame) will contain 525 scan-lines, which will be scanned in 1/30 second. Each frame is generated by interlacing two fields, each containing 262.5 scan-lines, which is produced in 1\60 second. If the vertical blanking interval — the time required for the scanning electron beam (in a video tube) to reposition itself from the bottom of one field to the top of the next — is taken into account, vertical resolution of NTSC video is limited to about 242 lines per field. Horizontal resolution is the amount of detail in the horizontal direction of the picture and is dependent primarily on the frequency bandwidth of the video signal.It is expressed as the number of lines that can be resolved in three-quarters of the picture width — a function of the 4:3 aspect ratio of video. For broadcast television, this bandwidth is fixed by the FCC (each channel is allocated a 6-MHz bandwidth). In remote sensing applications, the videographic imagery is generally not collected for broadcast purposes. In this context, the horizontal resolution of the data is determined by the quality of the video camera/lens system and the video cassette recorder.

The faster the magnetic tape can be moved across the gap of the recording head, the better the recording of high-frequency (i.e. rapidly varying) signals will be. Clearly, increasing the tape speed in order to record a 4-MHz signal would require an unrealistic amount of tape. This problem was solved by radically changing the tape scanning method. Whereas audio tape is pulled past a stationary recording head, video tape is usually moved past a rapidly rotating head. Hence, the relative tape speed is dramatically increased without using a prohibitive amount of tape.

The frequency-modulated video signal, called the luminance or Y signal, carries the black and white information of the scene. This achromatic data provides the spatial detail in the video image. The color information in the video signal, the chrominance (or chroma) signal, is converted by the VCR to a lower-frequency, non-modulated subcarrier. Two different color subcarrier frequencies are used, depending on the recording format.

3.4 VCR Formats

The portable VCR technology required for airborne videography is barely twenty years old. Sony introduced the 3/4-inch U-Matic format in 1969, and within three years it became the industrial standard. The 1/2-inch "consumer" formats, Beta and VHS, both were released in the late '70s. Beta was the second format which

c 1999 David P. Lusch, Ph.D.

Sony marketed — hence their use of the second letter of the Greek alphabet to name the product. Originally, VHS stood for Vertical Helical Scan, a studio recording method. Later, VHS became a trademark of JVC, Inc as the Video Home System. These product names have now been extended in usage to represent two different, and unfortunately incompatible, video formats. In early 1987, Sony improved their 3/4-inch product line with the addition of the 3/4-inch SP U-Matic. Later that same year, JVC released a much-improved 1/2-inch format called Super VHS (S-VHS). Sony produced the newest professional format in 1988: Extended Definition (ED) Beta.

In addition to these consumer-grade and industrial formats, the early '80s saw the introduction of professional component recorders. Sony developed the Betacam system, whereas Panasonic and RCA supported the M-format. These very expensive recorders use tape at six times the normal speed in order to record the chrominance signals separately from the luminance signal. Yet another professional format was released by Panasonic in 1985 — the VHS-based M-2 format. This special type of recorder uses metal-particle tape and is known for providing superb reproductions out to several generations. To date, these professional systems, mostly because of their cost, have not been used much in video remote sensing.

As mentioned earlier, the vertical resolution of video is determined primarily by the fixed number of interlaced scan lines. The horizontal resolution, in comparison, is determined in large part by the maximum recording frequency. Figure 3.2 shows that the 1/2-inch, VHS format uses a peak frequency of 4.4 MHz (Beta uses 4.8 MHz). This provides a maximum recorded horizontal resolution of about 240 lines, regardless of how many lines the video camera produced. The 3/4-inch, U-Matic format has a 5.4 MHz peak frequency which allows about 260 vertical lines to be recorded. With their 3/4-inch, SP U-Matic format, Sony provided a major improvement in recordable resolution. In this format, the peak recording frequency is 6.6 MHz, providing 340 lines of horizontal resolution. The S-VHS format boosts the peak recording frequency to 7.0 MHz, providing more than 400 lines of horizontal resolution. ED Beta uses a peak frequency of 9.3 MHz. It's reported to be able to reproduce about 500 lines of resolution.

In order to use these higher signal frequencies, which are more difficult to record, improved types of magnetic tape were required. The more magnetically absorbent a tape is, the easier it is to record a high-frequency signal. Magnetic absorbency is called coercivity and is measured in oersteds. Standard VHS tape has a coercivity of about

© 1999 David P. Lusch, Ph.D.

Video Bandwidths

3.2

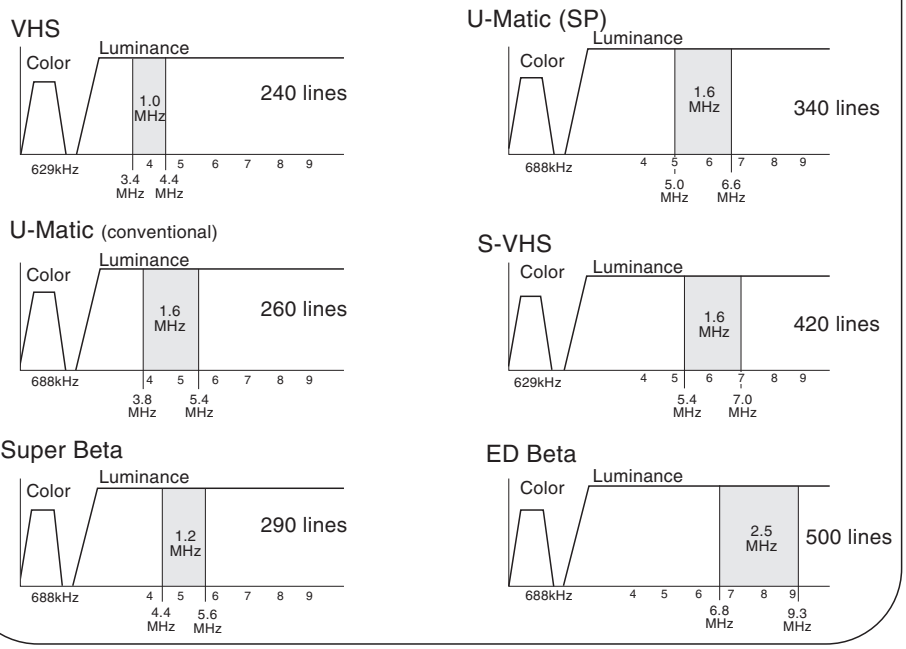

c 1999 David P. Lusch

700 oersteds. The 3/4-inch formats, U-Matic and the SP U-Matic, have tape coercivities of around 650 and 720 oersteds, respectively. The S-VHS tape has a coercivity of at least 900 oersteds. The ED Beta system shifted to a metal tape having a coercivity of about 1450 oersteds.

The frequency bandwidth of the recorded video signal is analogous to the quantization level of a digital system. The larger the dynamic range, the better small reflectance differences in the scene can be recorded. With a broader frequency bandwidth, the system electronics in a VCR are better able to discriminate between closely-grouped frequencies associated with minor differences in scene brightness. This increased contrast helps to sharpen the appearance of the image.

Standard VHS has a 1.0 MHz luminance-signal bandwidth (see Figure 3.2). Black is recorded as a 3.4 MHz frequency and white is recorded as a 4.4 MHz signal. The S-VHS and the two U-Matic formats use a 1.6 MHz luminance-signal bandwidth. In the case of Super VHS, white is recorded as a 7.0 MHz signal while black is recorded as a 5.4 MHz frequency. ED Beta uses a 2.5 MHz bandwidth ranging from 6.8 MHz (black) to 9.3 MHz (white).

Both the S-VHS and ED Beta VCRs are capable of recording and playing back the luminance (Y) signal separately from the chrominance (C) signal. This avoids the mixing of these two signals inherent to the NTSC format. The separated Y/C signals can be displayed on special monitors. The results are TV pictures which appear somewhat sharper because the color component is more crisply displayed, especially along the edges of features.

3.5 Color Infrared Videography

A standard color video camera using vidicon tubes as its sensor is shown in Figure 3.3. Like all multispectral imaging devices, the camera decomposes the incoming radiant energy into three separate spectral paths and provides a separate detector for each channel. In the example shown here, dichroic mirrors are used for the beam splitter. These optical devices have preferred reflectivity — the "blue" mirror, for example, reflects bluish wavelengths of light, but freely transmits the greenish and reddish light. Other methods, such as prisms, can also be used as the beam splitter.

In the spring of 1983, researchers at the University of Minnesota developed the first single-camera, color infrared video

© 1999 David P. Lusch, Ph.D.

Video Cameras

3.3

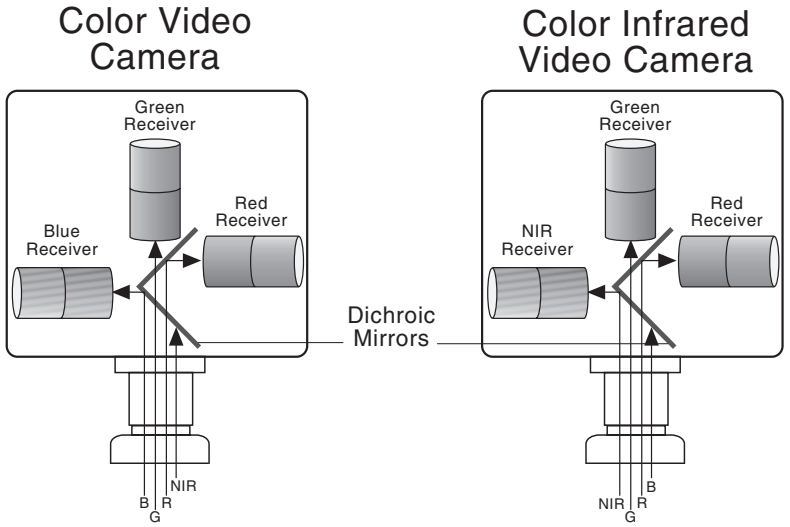

c 1999 David P. Lusch

system (Meisner and Lindstrom, 1985). Two major modifications of a standard, three-tube, color video camera were made. First, the beam-splitter assembly was replaced with one that rejects blue light altogether, but separates the green, red and near infrared components using different dichroic mirrors (Figure 3.3). Second, the Saticon tube and its supporting electronics from the blue channel were removed and replaced with a silicon target tube which has sensitivity in the near infrared portion of the spectrum (Figure 3.4). This camera still produces a standard NTSC composite signal, so standard video cassette recorders can be used to capture the imagery.

3.6 Airborne Videography

Research into the possible applications of video from aircraft (now generally referred to as videography) began in the late 1960s, but flourished in the 1980s. Early pioneers in these endeavors include Robinove and Skibitzke (1967), Mozer and Seige (1971), Schumacher (1980), Edwards (1982), Manzer and Cooper (1982), Escobar et al. (1983), Mussakowsi (1983), Vlcek (1983), and Nixon et al. (1984). The best single compilation of information concerning videography and its numerous applications in agriculture, forestry, rangeland, soils, and water is the proceedings of the First Workshop on Videography (Mausel, 1988).

In striking parallel with the development path of aerial photography, airborne videography has moved through black and white, B/W infrared, color, and color infrared capabilities. Everitt (1988) provides a succinct review of the historical development of videography. Table 3.1 lists the major advantages and disadvantages of videography.

Most airborne videography, like aerial photography, is acquired in the vertical mode (Figure 3.5). This can be accomplished with a clamp-on exterior mount, but is best done using a belly mount so that the video camera is afforded some environmental protection. Other necessary pieces of equipment include a portable VCR and some means of powering the system (batteries or connection to the aircraft power system). A small portable video monitor is, while not a necessity, a great advantage to ensure that the system is working and that the flight line is correct. Meisner (1986) and Vlcek (1988) should be consulted for more information about planning an airborne videography mission.

© 1999 David P. Lusch, Ph.D.

Video Detectors 3.4

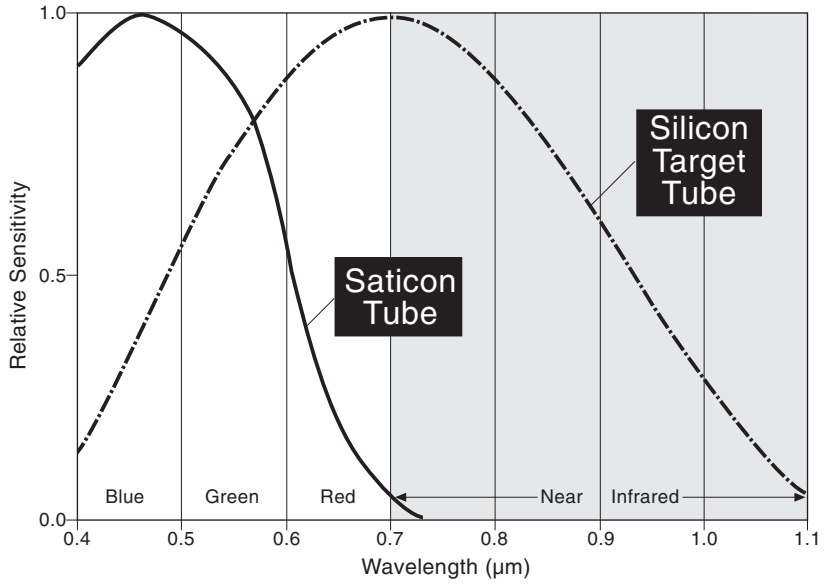

Airborne Videography 3.5

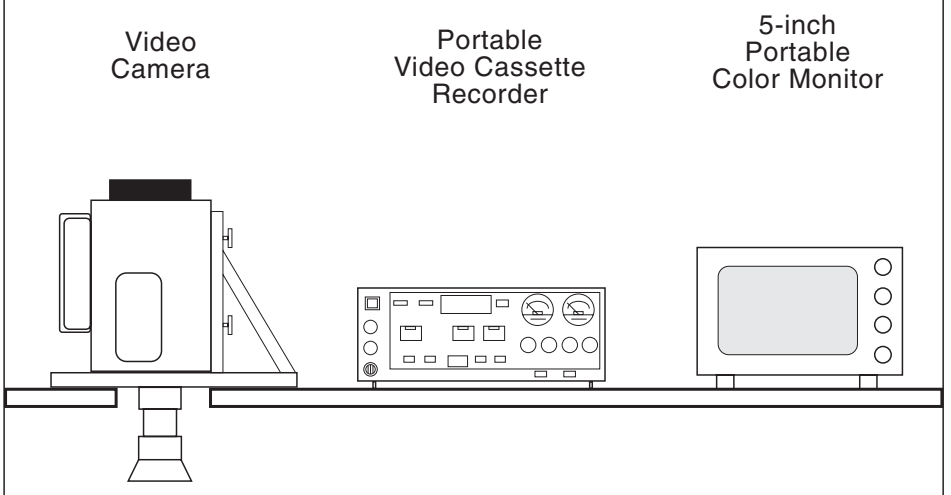

c 1999 David P. Lusch

Table 3.1 Advantages and Disadvantages of Videography

Advantages	Disadvantages
• Near-real-time availability of the imagery	• Low spatial resolution
• Greater light sensitivity than film permitting narrow band imagery and longer wavelength sensitivity	• Difficult to obtain hard copy of the images
	• Relatively narrow field of view
• Immediate potential for digital processing of the video signal	• Near-infrared video systems have a vignetting problem
• Equipment is portable, versatile, easy to use, and has a low operating cost	• Calibration is difficult due to automatic gain control
• Ability to view live imagery concurrent with its acquisition	
• Ability to record “field notes” on the audio track	
• High frame rate (30 per second) offers extreme endlap which can be useful in some situations (e.g. small, scattered clouds below the aircraft)	

© 1999 David P. Lusch, Ph.D.

References

Edwards, G.J. 1982. Near-infrared aerial video evaluation for freeze damage. *Proc.Florida State Horticulture Society.* v. 95, pp. 1-3.

Escobar, D.E., R.L. Bowen, H.W. Gausman, and G.R. Cooper. 1983. Use of near-infrared video recording system for the detection of freeze-damaged citrus leaves. *J. Rio Grande Valley Horticulture Society.* v. 36, pp. 61-66.

Everitt, J.H. 1988. Introduction to videography: Historical overview, relation to remote sensing, advantages, disadvantages. *Proc. First Workshop on Videography.* Falls Church, VA: American Society of Photogrammetry and Remote Sensing. pp. 1-4.

Manzer, F.E. and G.R. Cooper. 1982. Use of portable video-taping for aerial infrared detection of potato disease. Plant Disease. 66: 665-667.

Mausel, P. W.(ed.). 1988. First Workshop On Videography. Falls Church, VA:American Society of Photogrammetry and Remote Sensing. 270p.

Meisner, D.E. 1986. Fundamentals of airborne video remote sensing. *Remote Sensing of Environment.* v. 19: 63-79.

Meisner, D.E. and O.M. Lindstrom. 1985. Design and operation of a color infrared aerial video system. *Photogrammetric Engineering and Remote Sensing.* v.51, no. 5 (May), pp. 555-560.

Mozer, M. and P. Seige. 1971. High resolution multispectral TV camera system. Proc. 7th International Symposium on Remote Sensing of Environment. pp. 1475-1481.

Mussakowski, R.S. 1983. The application of video remote sensing to resource surveys and environmental monitoring. Proc. 8th Canadian Symposium on Remote Sensing. pp. 91-99.

c 1999 David P. Lusch, Ph.D.

Nixon, P.R., D.E. Escobar, R.L. Bowen, and A.J. Richardson. 1984. Video color-infraredimagery: a future natural resource tool. *Proc. 9th Biennial Workshop on Color Aerial Photography in the Plant Sciences.* Falls Church, VA: American Society of Photogrammetry. pp. 159-164, 204.

Robinove, C. and H. Skibitzke. 1967. An airborne multispectral television system. U.S.Geological Survey Professional Paper 575-D. pp. D143-D146.

© 1999 David P. Lusch, Ph.D.

(c) 1999 David P. Lusch, Ph.D.

Chapter 4	Multispectral Scanner Systems

Contents

© 1999 David P. Lusch, Ph.D.

4.1 Objectives

- Define the term "pixel".
- Define the term "Digital Number (DN)".
- Explain the difference between IFOV and ground resolution.
- Describe the cause of geometric distortion from scanners.
- Compare imaging spectrometers to multispectral scanners.
- Explain the necessity of using polar-orbiting satellites for earth-resources observations.
- List the spectral sensitivities of the eight Landsat-7 ETM+ bands.
- Describe the potential information content of each spectral band of the Enhanced Thematic Mapper.
- Given a set of generalized spectral reflectance curves for selected features, predict the display color which will form using several different RGB band combinations.
- Compare the spatial, spectral, and revisit differences between Landsat-7 and SPOT-4.
- List the advantages of the off-nadir viewing capability of SPOT-4.
- List the spatial, spectral, and revisit characteristics of the AVHRR instrument on the NOAA Polar Orbiter satellites.
- Define the vegetation index concept and describe its use.

4.2 Introduction

Basic concepts of digital image data are presented to introduce the topic of scanning systems, their geometric distortions and the difference between imaging spectrometers and multispectral scanners. Satellite multispectral scanners are introduced with a comparison of the Landsat 7 ETM+ instrument and the HRVIR imager on SPOT 4. For historical completeness, the first- and second-generation Landsats (1-3 and 4-5) and the first SPOT series (1-3) are also described. The AVHRR instrument is briefly discussed and compared with the current Landsat and SPOT systems.

© 1999 David P. Lusch, Ph.D.

4.3 Multispectral Scanners

Scanning Systems

There are two approaches used "scan" an image from a remote platform. The first, across-track scanning, uses a rotating or oscillating mirror to sweep one or more detectors across the scene while the platform carries the imager along the flight tract (Figure 4.0a). The alternative method - along-track scanning- uses a fixed, linear array of numerous detectors which form the physical width of the scene. Each detector forms one column of data. Again, the platform motion develops the length of the image (Figure 4.0b). Notwithstanding these differences, all imagers have three hardware components in common : front-end optics, beam splitter and analog-to-digital converter (Table 4.1).

Concepts of Digital Image Data

• *Pixel* is a contraction of picture element, which is the area or cell from which radiance or landscape brightness is recorded by a multispectral scanner. (Note, the assigned pixel dimensions may not exactly correspond to the area from which the radiance measurements were made (i.e. the IFOV) if the system "over scans" - this was the case with the MSS instrument on Landsats 1-3).

• *Digital Number* (DN) is the relative radiance measurement or "brightness" value (BV), recorded as an integer, for an individual pixel in an individual spectral band.

• *IFOV* (instantaneous field-of-view) is the solid angle subtended by a detector element in an imaging device when the scanning motion is stopped. The IFOV is a system specification, usually presented in radians, milliradians or microradians.

• *Ground resolution* refers to the area of the earth's surface captured by the IFOV of a radiometer at a given flying height above the terrain:

$$D = H' \beta$$

where D = diameter of the ground area viewed
H' = flying height above the terrain
β = IFOV of the system expressed in radians

© 1999 David P. Lusch, Ph.D.

Across-track or Whiskbroom MSS system operation

4.0a

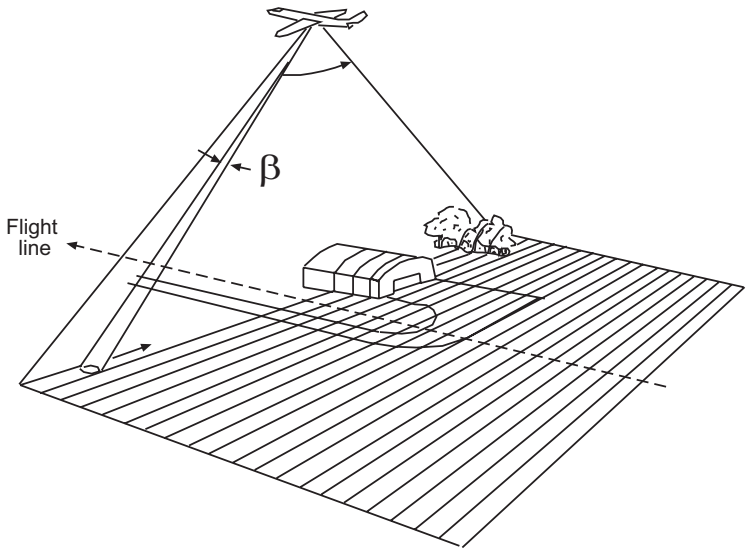

Along-track or Pushbroom MSS system operation

4.0b

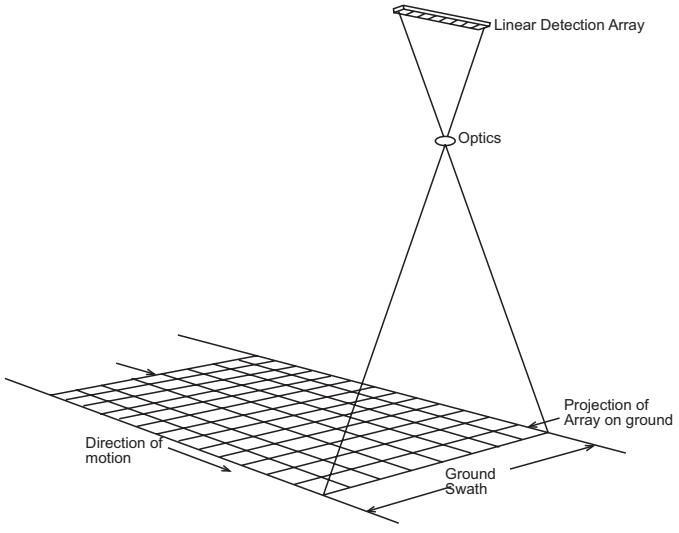

c 1999 David P. Lusch, Ph.D.

TABLE 4.1 COMMON COMPONENTS OF MULTISPECTRAL SCANNERS

1. SCANNING METHODS

- Across - Track Scanning (Whiskbroom)
- Along - Track Scanning (Pushbroom)

2. HARDWARE BASICS

- COLLECTION OPTICS
  - Includes the scan mirror for across-track scanners
  - Determines the field-of-view (i.e. total image width)
  - For a given detector size and flight altitude, determines the ground resolution
- BEAM SPLITTER
  - Decompose incoming radiance into separate wavelength ranges (bands)
  - Uses dichroic gratings, dichroic mirrors, or prisms
- ANALOG-TO-DIGITAL CONVERTER
  - Analog = continuous signal
  - Digital = sampled signal
  - Radiometric Resolution (number of recorded radiance levels)
    - $2^6 = 64$; $2^8 = 256$; $2^{10} = 1024$
  - Recorder and/or Transmitter
    - for Landsat 7:
      - recorder = 350 Gb solid-state memory
      - transmitter = X-Band @ 150 Mbs

© 1999 David P. Lusch, Ph.D.

Geometric Distortion

The causes of geometric distortion from scanners include:

- variations in the altitude, attitude, and velocity of a sensor's platform
- skew distortions due to the rotation of the Earth beneath the sensor during imaging
- displacement due to relief and curvature of the Earth
- inconsistent velocity of the sweep of the scanner mirror (across-track systems only)

Imaging Spectrometers

- *Imaging spectrometers* are instruments which acquire images in many, very narrow, spectral bands. These instruments have been used almost exclusively for research about spectral reflectance and target discrimination, but are becoming more commonly available - e.g. MODIS on Terra (formerly EOS AM-1).

- *Multispectral scanners*, like imaging spectrometers, produce several spectrally distinct images, but the bandpasses tend to be rather wide and the total number of bands is small (usually less than 10).

c 1999 David P. Lusch, Ph.D.

Practicum - Angular Resolving Power
Comparing your Eye to Landsat and SPOT

The resolving power of your eyes can be determined by viewing resolution targets from a fixed distance (say 5 meters). The worked example below shows the results of a typical image interpreter.

High-Contrast Target	**Low-Contrast Target**
6 line-pairs cm^{-1}	***3*** line-pairs cm^{-1}
0.2 or 0.3 line width (mm)	***0.6*** line width (mm)

The spacing of these resolution targets is expressed in line-pairs per centimeter. The "line pair" is composed of a black bar immediately flanked by a white bar of the same width.

So, for a target with 3 line-pairs cm^{-1}, each individual bar must be

1.67 millimeters wide.

3 line-pairs = 6 lines ***1 cm = 10 mm*** ***10 mm / 6 lines = 1.67 mm/line***

For our example result above, resolving 6 line-pairs per cm, each line is

0.83 mm wide

6 line-pairs = 12 lines ***1 cm = 10 mm*** ***10 mm / 12lines = 0.83mm/line***

We are all familiar with the system of measuring plane angles in degrees, but the unit of angular measure in the International System of Units (SI; the so-called metric system) is the **radian (rad)**.

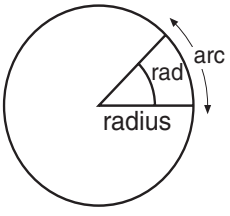

The radian is that unique angle which subtends an arc length which is just equal to the radius of a circle.

$$1 \text{ rad} = \frac{\text{arc length}}{\text{radius}}$$

© 1999 David P. Lusch, Ph.D.